

# **METTL3 regulates heterochromatin in mouse embryonic stem cells**

Wenqi Xu<sup>1,2</sup>, Jiahui Li<sup>1</sup>, Chenxi He<sup>1</sup>, Jing Wen<sup>1</sup>, Honghui Ma<sup>1</sup>, Bowen Rong<sup>1</sup>, Jianbo Diao<sup>1</sup>,  
Liyong Wang<sup>1</sup>, Jiahua Wang<sup>1</sup>, Feizhen Wu<sup>1</sup>, Li Tan<sup>1</sup>, Yujiang Geno Shi<sup>3</sup>, Yang Shi<sup>4,\*</sup>, Hongjie  
Shen<sup>1,\*</sup>

<sup>1</sup>Center for Medical Research and Innovation, Shanghai Pudong Hospital, Fudan University  
Pudong Medical Center, and the Shanghai Key Laboratory of Medical Epigenetics, the  
International Co-laboratory of Medical Epigenetics and Metabolism, Ministry of Science and  
Technology, Institutes of Biomedical Sciences, Fudan University, 2800 Gongwei Road,  
Pudong, Shanghai 201399, China.

<sup>2</sup>Key Laboratory of Carcinogenesis and Cancer Invasion, Ministry of Education, Liver Cancer  
Institute, Zhongshan Hospital, Fudan University, Shanghai, 200032, China.

<sup>3</sup>Division of Endocrinology, Diabetes and Hypertension, Department of Medicine, Brigham  
and Women's Hospital, Harvard Medical School, Boston, MA 02115, USA.

<sup>4</sup>Ludwig Institute for Cancer Research, Oxford Branch, Oxford University, UK

\*Correspondence:

yang.shi@ludwig.ox.ac.uk (Y.S.)

hongjieshen@fudan.edu.cn (H.S.)

METTL3 (methyltransferase-like 3) mediates mRNA N<sup>6</sup>-methyladenosine (m<sup>6</sup>A) methylation, which impacts mRNA stability and protein translation<sup>1</sup>. METTL3 has also been shown recently to bind chromatin<sup>2-4</sup>, but the role of METTL3 and m<sup>6</sup>A methylation in the chromatin context is not fully understood. Here we report a direct role of METTL3 in regulating heterochromatin in mouse embryonic stem cells (mESCs), whose integrity is critical for silencing retroviral elements and for mammalian development<sup>5</sup>. We demonstrate that METTL3 predominantly localizes to the intracisternal A particles (IAPs)-type endogenous retroviruses family. Importantly, *Mettl3* knockout impairs deposition of multiple heterochromatin marks onto METTL3-targeted IAPs, and upregulates IAP transcription, suggesting that METTL3 is important for IAP heterochromatin integrity. We provide further evidence that RNA transcripts derived from METTL3-bound IAP-types are associated with chromatin and are m<sup>6</sup>A methylated. These m<sup>6</sup>A-marked transcripts are bound by the m<sup>6</sup>A reader YTHDC1, which interacts with METTL3 and in turns promotes METTL3 chromatin association. Additionally, METTL3 also physically interacts with the H3K9 tri-methyltransferase SETDB1 and co-factor TRIM28 and is important for their localization to IAPs. Taken together, our findings demonstrate that METTL3-catalysed RNA m<sup>6</sup>A modification is important for IAP heterochromatin integrity in mESCs, thus revealing a novel mechanism of heterochromatin regulation in mammals.

To understand the function and mechanism of action of METTL3 in chromatin regulation in mESCs, we first interrogated METTL3 chromatin localizations and their association with

heterochromatin and euchromatin histone marks, respectively. We found that out of a total of 1,928 METTL3 binding events (based on uniquely mapped reads only), a majority of them are associated with the two heterochromatin marks, H3K9me3 (90.0%, 1,735/1,928) and H4K20me3 (91.5%, 1,764/1,928), respectively, but METTL3 is rarely associated with the H3K27me3 repressive mark (0.4%, 8/1,928) or the euchromatin mark, H3K4me3 (5.1%, 98/1,928). METTL3 has previously been reported to bind promoters of coding genes in cancer cell lines<sup>3,4</sup>. Consistently, we found a small percentage of METTL3 peaks mapped to promoters (1.5%, 28/1,928) in mESC, but this percentage increased significantly upon differentiation of mESCs to embryoid bodies (EBs) (46.4%, 1,595/3,434). We further calculated the overlapping ratios (Jaccard statistics, see Methods) and relative distances between METTL3 binding sites and the peaks of histone modifications, both of which suggest a strong association between METTL3 and H3K9me3/H4K20me3 (Fig. 1a and Extended Data Fig. 1a). Their co-enrichment is further shown in the heatmap in Fig. 1b. These observations suggest that METTL3 may play a role at heterochromatin in mESCs.

Heterochromatin establishment and maintenance are critical for gene regulation and genome integrity<sup>6</sup>. In mammals, constitutive heterochromatin formed over repetitive elements including endogenous retroviruses (ERVs), such as IAP (intracisternal A-type particle), which are decorated by H3K9me3 and H4K20me3<sup>7</sup>. H3K9me3 is mediated by the methyltransferase SETDB1 (ESET or KMT1E) and its regulator TRIM28 (KAP1), both of which play a prominent role in IAP silencing in mESCs<sup>8,9</sup>. H4K20me3 is mediated by Suv4-20H1/2 and generally requires H3K9me3 for its deposition<sup>10</sup>. METTL3 binding events are mainly enriched

on ERVK elements ([Extended Data Fig. 1b-c](#)), which are decorated by H3K9me3 and H4K20me3, respectively ([Extended Data Fig. 1d](#)). A strong positive correlation between averaged METTL3 enrichment and those of H3K9me3 or H4K20me3 ([Extended Data Fig. 1e](#)) reveals co-enrichment of METTL3 and H3K9me3/H4K20me3 on specific subtypes of ERVK. Specifically, METTL3 appears to mostly bind the IAP elements, especially the IAPez subtype, including the internal region of IAPez (IAPez-int) and the flanking cognate Long Terminal Repeats (LTRs) ([Fig. 1c](#)). In addition to the intact IAPez-int elements with lengths over 6 Kb, many truncated IAPez-int fragments are also defined as individual IAPez-int elements in the Repeatmasker database, which might cause an over-representation of their total numbers. To reduce this bias, we stitched the adjacent IAPez-int fragments and defined a total number of 2,542 IAPez-int elements for further investigation ([Extended Data Fig. 1f](#)). We found METTL3 binding densities positively correlated with those of H3K9me3 ([Fig. 1d](#)) and H4K20me3 ([Fig. 1e](#)) on IAPez-int elements. Furthermore, METTL3 is enriched throughout the entire body of IAPez-int, similar to the distributions of H3K9me3 and H4K20me3, but with a stronger binding to the 5' end than the 3' end ([Extended Data Fig. 1g and Fig. 1f](#)). The specific binding of METTL3 to IAPez, but not other retrotransposons was validated by ChIP-qPCR using three different METTL3-specific antibodies ([Extended Data Fig. 1h](#)). Using either unique-only or unique+random mapping strategies ([Extended Data Fig. 1i](#)), we reached the same conclusion of co-enrichment of METTL3 with H3K9me3 and H4K20me3 over ERVKs in mESCs ([Extended Data Fig. 1j](#)). In order to display both site-specific and global features on repetitive elements, unique-only reads (for analyses on individual sites) and unique+random reads (for averaged analyses on repetitive elements classes) are both used in this study (see

Figure Legends and Methods).

IAPEz-int is primarily controlled by H3K9me3 in mESCs<sup>8,9</sup>. To investigate the functional significance of METTL3 enrichment over IAP elements, we first generated and validated *Mettl3* KO and rescued cells containing either wildtype or catalytically compromised METTL3, METTL3<sup>APPA</sup> (DPPW motif mutated to APPA)<sup>11</sup>([Extended Data Fig. 2a-b](#)). Importantly, we observed a significant decrease of the H3K9me3 and H4K20me3 levels on IAPEz-int elements in the *Mettl3* KO cells, which was restored by METTL3<sup>WT</sup>, but not METTL3<sup>APPA</sup> ([Fig. 2a-b](#), [and Extended Data Fig. 2c-e](#)), suggesting that METTL3 regulates heterochromatin states on IAPEz-int via its catalytic activity. Consistently, depleting the m<sup>6</sup>A demethylase, ALKBH5<sup>12</sup>, led to a significant increase of H3K9me3 ([Extended Data Fig. 2f-i](#)). We found down-regulation of H3K9me3 and H4K20me3 upon *Mettl3* KO is restricted to the METTL3-targeted IAPs, but not non-IAP ERVK or other types of repetitive elements, which are otherwise not bound by METTL3 ([Extended Data Fig. 2j-k](#)). Similarly, IAP-enriched histone variant H3.3<sup>13</sup> and DNA methylation<sup>14</sup> important for transposon silencing were reduced upon *Mettl3* KO, and were rescued by METTL3<sup>WT</sup>, but not METTL3<sup>APPA</sup> ([Extended Data Fig. 3a-b](#)). Down-regulation of H3.3 upon *Mettl3* KO is restricted to the METTL3-targeted IAPs ([Extended Data Fig. 3c](#)) but down-regulation of DNA methylation in the *Mettl3* KO cells is not ([Extended Data Fig. 3d](#)), suggesting that METTL3 regulates DNA methylation via multiple mechanisms. Collectively, these findings suggest that METTL3 loss compromises heterochromatin integrity.

By carrying out total RNA-seq, we observed a significant up-regulation of IAPEz-int transcription upon *Mettl3* KO, which was suppressed by re-introduction of METTL3<sup>WT</sup>, but not METTL3<sup>APPA</sup> (Fig. 2c and Extended Data Fig. 3e). Furthermore, de-repression upon METTL3 loss is specific to IAPs (Extended Data Fig. 3f). The IAPEz-int RNA transcript level is negatively correlated with the densities of METTL3, H3K9me3 and H4K20me3 (Extended Data Fig. 3g-i) but not DNA methylation (Extended Data Fig. 3j), which does not play a dominant role in IAP silencing in mESC<sup>8</sup>. As METTL3 is known to regulate RNA stability<sup>15</sup>, we next determined and compared the stability of the transcript level of IAPEz-int with that of the coding gene, *Nxtl*, in the presence and absence of METTL3 at different time points post Actinomycin D treatment, which blocks transcription. As expected, degradation of the *Nxtl* mRNA was severely impaired in the absence of METTL3 (Fig. 2d, Right), but the stability of the IAPEz-int RNAs remained unaltered (Fig. 2d, Left). Furthermore, re-analysis of the published RNA-seq data<sup>16</sup> showed no increase of the IAP RNA levels in cells depleted of all three YTHDF proteins (YTHDF1/2/3) (Extended Data Fig. 3k), which are the m<sup>6</sup>A readers reported to regulate RNA decay<sup>16,17</sup>. Taken together, these results suggest that METTL3-mediated suppression of IAPEz-int is likely at the chromatin level.

In order to elucidate the mechanism by which METTL3 regulates IAPEz-int, we first compared METTL3 enrichment on METTL3-bound IAPEz-int elements in parental, *Mettl3* KO and the two rescued cell lines. As expected, METTL3 enrichment on IAPEz-int was abolished in the *Mettl3* KO cells and was restored by reintroducing METTL3<sup>WT</sup>. Surprisingly, METTL3<sup>APPA</sup> and two additional METTL3 catalytic mutants, METTL3<sup>W475A</sup> and METTL3<sup>N477A</sup> (which

134 disrupt the loop required for fencing catalytic cavity between METTL3 and METTL14)<sup>18</sup> all  
135 failed to localize to these repetitive elements, suggesting that association of METTL3 with  
136 chromatin may be dependent on its own catalytic activity (Fig. 3a-b, and Extended Data Fig.  
137 4a-e). We also found depletion of METTL14 and other components of the METTL3/METTL14  
138 methyltransferase complex reduced METTL3 chromatin association (Extended Data Fig. 4f-  
139 k). In contrast, dCas9-guided, ectopically placed METTL3<sup>WT</sup> or METTL3<sup>APPA</sup> at IAPs in  
140 *Mettl3* KO cells both induced H3K9me3 (Extended Data Fig. 4l-n). This indicates that once  
141 successfully localized to a specific chromatin location, METTL3 has the ability to regulate  
142 H3K9me3 installment independent of its catalytic activity.

143  
144 We next asked how METTL3 regulates H3K9me3 and heterochromatin formation. H3K9me3  
145 at IAPez-int is regulated by the SETDB1 methyltransferase and the associated factor  
146 TRIM28<sup>8,9</sup>. Interestingly, TRIM28 was recently reported to interact with METTL3<sup>19</sup>.  
147 Consistently, we found significant overlaps of the TRIM28 and SETDB1-bound IAPez-int  
148 elements with those bound by METTL3 (Extended Data Fig. 5a) and positive correlations  
149 between their binding densities on these elements (Extended Data Fig. 5b). Furthermore, we  
150 found that METTL3 is co-immunoprecipitated with both SETDB1 and TRIM28 (Fig. 3c).  
151 Consequently, we next investigated whether METTL3 regulates the recruitment of SETDB1  
152 and TRIM28 to IAPez-int elements. We carried out ChIP-seq of SETDB1 and TRIM28 and  
153 found a decrease of both SETDB1 and TRIM28 in *Mettl3* KO cells (Fig. 3d-e and Extended  
154 Data Fig. 5c-d), compared with the parental cells. Similar to H3K9me3, the decreased  
155 enrichment of SETDB1 is specific to IAP (Extended Data Fig. 5e). The decrease of TRIM28

is most pronounced on IAPs, although it is also modestly reduced on other types of repetitive elements (Extended Data Fig. 5f). We found that catalytic mutation of METTL3 or inhibition of transcription by and large did not significantly affect the interactions of METTL3 with SETDB1 and TRIM28 (Extended Data Fig. 5g). These findings suggest that METTL3 facilitates the IAP-localization of SETDB1/TRIM28 to regulate H3K9me3 on chromatin, possibly through physical interactions. In contrast, the catalytic activity of METTL3 appears to be only necessary for METTL3 binding onto chromatin but not recruitment of the H3K9me3 methyltransferase machinery.

Given that the catalytic activity of METTL3 is important for METTL3's association with the IAPEz repetitive elements, we hypothesized that m<sup>6</sup>A methylated transcripts at these locations may be important for METTL3 localization. Indeed, by fractionating whole cell extracts into cytosolic, soluble nuclear and chromatin fractions, followed by RT-qPCR, we found that a large proportion (~50%) of the IAPEz transcripts are associated with chromatin (Extended Data Fig. 6a). This finding is further confirmed by our ChIRP-seq (Extended Data Fig. 6b) and re-analysis of the published GRID-seq data<sup>20</sup> (Extended Data Fig. 6c). We next carried out MeRIP using chromatin total RNA to detect m<sup>6</sup>A on IAPEz transcripts and identified a total of 35,193 potential METTL3 dependent m<sup>6</sup>A peaks genome-wide, which contain the classic DRACH consensus sequences, supporting the idea that they are bona fide m<sup>6</sup>A peaks (Extended Data Fig. 6d). Consistent with the previous findings<sup>21,22</sup>, we showed that m<sup>6</sup>A enrichment on the 3' ends of the mRNAs from coding genes is abrogated in the *Mettl3* KO cells (Extended Data Fig. 6e-f). Interestingly, we found that METTL3 dependent m<sup>6</sup>A on the IAP transcripts is

specifically enriched on their 5' and not 3' ends (Fig. 4a-b) (a total of 104 m<sup>6</sup>A peaks localized to 86 IAPeZ elements). The ability of MeRIP-seq to detect m<sup>6</sup>A-marked transcripts may be limited when transcripts are expressed at a low level such as the IAPeZ transcripts, which can lead to under-estimation of the m<sup>6</sup>A level. Indeed, as SETDB1 depletion increases IAPeZ transcription<sup>8</sup>, MeRIP-seq in the *Setdb1* KO cells identified significantly increased m<sup>6</sup>A signals on the 5' ends of IAPeZ-int (a total of 752 m<sup>6</sup>A peaks localized to 527 IAPeZ elements) (Fig. 4c and Extended Data Fig. 6g-h). In order to rule out potential biases caused by the m<sup>6</sup>A antibody used in the MeRIP experiments, we further validated m<sup>6</sup>A modification on five adenosine sites residing at the 5' end of the IAPeZ-int consensus sequence using SELECT, which is an elongation and ligation-based quantitative PCR amplification method for the detection of m<sup>6</sup>A position at single-nucleoside resolution<sup>23</sup> (Fig. 4d). The five adenosine sites identified by SELECT include the canonical site GAA<sup>159</sup>CU, as well as non-canonical sites UAA<sup>107</sup>AG, UAA<sup>132</sup>GA, GAA<sup>135</sup>GG, GGA<sup>138</sup>UU. Both the canonical (GAACU)<sub>4</sub> and one of the non-canonical sites, (GGAUU)<sub>4</sub>, can be methylated by METTL3/METTL14 in vitro, although to a less extent compared with the most optimal motif, (GGACU)<sub>4</sub> (Extended Data Fig. 6i).

RNA m<sup>6</sup>A methylation is recognized by a family of proteins with a conserved YTH domain, which mediates recognition of m<sup>6</sup>A<sup>1</sup>. We found that the nuclear m<sup>6</sup>A reader, YTHDC1<sup>24</sup>, is localized to IAPeZ-int elements (Extended Data Fig. 7a). ChIP-seq showed a significant overlap between the binding sites of METTL3 and YTHDC1 (Extended Data Fig. 7b) and a significant positive correlation between their binding densities on IAPeZ-int elements

(Extended Data Fig. 7c), suggesting a possible interplay between the m<sup>6</sup>A writer and reader on IAPez-int. Supporting this hypothesis, we identified a significant reduction of YTHDC1's chromatin association in the *Mettl3* KO cells, which was rescued by METTL3<sup>WT</sup>, but not METTL3<sup>APPA</sup>. (Fig. 4e and Extended Data Fig. 7d-e), suggesting that YTHDC1 binding to chromatin is dependent on RNA m<sup>6</sup>A methylation.

Given that YTHDC1 KO is cell lethal<sup>25</sup>, to further investigate whether m<sup>6</sup>A recognition is necessary for YTHDC1 binding to IAPez, we generated three cell lines, all of which carry an integrated, AID-tagged YTHDC1, but differ on whether their endogenous *Ythdc1* is wildtype (YTHDC1<sup>WT</sup>), a mutant for binding m<sup>6</sup>A (YTHDC1<sup>W429A</sup>)<sup>24</sup> or completely knocked out (*Ythdc1* KO) (Extended Data Fig. 7f). These cells also express the Auxin receptor TIR1, thus the addition of the Auxin analog IAA can induce degradation of the AID-tagged YTHDC1 (Extended Data Fig. 7g). We found significant downregulation of YTHDC1 binding on IAPez in the YTHDC1<sup>W429A</sup> and *Ythdc1* KO cell lines (Extended Data Fig. 7h-k). Supporting these findings, inhibition of transcription using a number of different transcription inhibitors also led to a significant reduction of YTHDC1 binding (Extended Data Fig. 7l).

Given that METTL3 recruitment requires its m<sup>6</sup>A catalytic activity, we next asked whether YTHDC1 reciprocally contributes to METTL3 binding. Indeed, METTL3 binding is significantly impaired in the YTHDC1<sup>W429A</sup> and the *Ythdc1* KO cells (Fig. 4f and Extended Data Fig. 8a-c). Accompanying the loss of METTL3 binding, we also observed significant

downregulation of H3K9me3 (Fig. 4g and Extended Data Fig. 8d-f) and H4K20me3 (Extended Data Fig. 8g-j) on IAPez-int. Furthermore, transcription from IAPez-int is significantly increased in both YTHDC1<sup>W429A</sup> and *Ythdc1* KO cells, consistent with an impaired heterochromatin in these cells (Fig. 4h). The reduction of H3K9me3 at IAPez-int is not further exacerbated by depletion of YTHDC1 in the *Mettl3* KO cells (Extended Data Fig. 8k-l), suggesting that METTL3 and YTHDC1 act in the same pathway to regulate heterochromatin on IAPez-int elements. In addition, artificially tethering YTHDC1 to IAPez by a CRISPR-based technology fails to restore H3K9me3 on these elements in *Mettl3* KO cells (Extended Data Fig. 8m-n), suggesting that YTHDC1 itself is not sufficient to induce heterochromatin formation. However, tethering YTHDC1 to IAPez in the *Mettl3* KO cells expressing the catalytic mutant, METTL3<sup>APPA</sup>, induces a significant H3K9me3 increase on IAPez (Extended Data Fig. 8o-p). Interestingly, we found METTL3 physically interacts with YTHDC1 (Fig. 4i), and this interaction is independent of transcription and the METTL3 catalytic activity (Extended Data Fig. 8q), suggesting a potential biochemical mechanism for the observed functional relationship between YTHDC1 and METTL3 in the recruitment of SETDB1/TRIM28 and regulation of IAP heterochromatin. Reciprocally, SETDB1 is also necessary for a stable association of METTL3 (Extended Data Fig. 9a-d) and YTHDC1 (Extended Data Fig. 9e-h) with IAPez. Taken together, we propose that m<sup>6</sup>A methylation by METTL3 provides a binding site for YTHDC1, which in turn recruits more METTL3 through physical interaction, forming a positive feedback loop that reinforces each other's localization to the IAPez regions (Extended Data Fig. 10a). The IAPez transcript-bound METTL3 recruits the H3K9 methyltransferase SETDB1/TRIM28 also through protein-protein interactions to

install H3K9 trimethylation at these repetitive elements. The interactions of the METTL3 complex with SETDB1/TRIM28 similarly reinforce their respective occupancies at these genomic regions, revealing yet another layer of positive feedback loop, which ensures heterochromatin integrity. These positive feedback loops are reminiscent of the multiple feedback loops identified in *S. pombe* heterochromatin assembly<sup>26</sup> (Extended Data Fig. 10b). Additionally, small RNAs are featured prominently in heterochromatin regulation in *S. pombe*<sup>26</sup>, raising the question of whether small RNAs are also involved in IAPEz heterochromatin regulation. In this context, a recent study in mESCs suggested endo-siRNAs in repetitive element repression in response to the loss of DNA methylation<sup>27</sup>.

Lastly, H3K9 methylation at *S. pombe* meiotic genes, interestingly, involves not only the RNAi-dependent mechanism central to constitutive heterochromatin, but also a YTH domain-containing protein Mmi1<sup>28</sup> (Extended Data Fig. 10c). Mmi1 has been shown to interact with additional factors and link RNA recognition to H3K9 methylation and possibly the assembly of facultative heterochromatin at meiotic genes<sup>28</sup>. As discussed earlier, YTH domains in mammals have been shown to function as an RNA m<sup>6</sup>A reader modality. However, the YTH domain in Mmi1 does not bind m<sup>6</sup>A<sup>29</sup> but rather recognizes the DSR (Determinant of Selective Removal) consensus motif on the RNAs transcribed from meiotic gene locus<sup>30</sup>, consistent with the fact that *S. pombe* lacks m<sup>6</sup>A due to the absence of the m<sup>6</sup>A enzyme, METTL3/METTL14<sup>11</sup>. Importantly, we showed that the YTH domain in YTHDC1 is required for YTHDC1-mediated heterochromatin regulation on IAPEz-int in mESCs (Fig. 4 and Extended Data Fig. 8). Thus, the strategy of RNA recognition for H3K9 methylation at heterochromatic regions appears to

be conserved in mammalian ESCs, although the exact molecular mechanisms are different.

Collectively, our findings identified a previously unappreciated yet crucial function of METTL3 and m<sup>6</sup>A methylation in heterochromatin regulation in mammalian embryonic stem cells and revealed potential underlying mechanisms, thus providing important insight into not only m<sup>6</sup>A function but also mechanisms of heterochromatin regulation in mammals.

## References:

- <sup>1</sup> Shi, H., Wei, J. & He, C., Where, When, and How: Context-Dependent Functions of RNA Methylation Writers, Readers, and Erasers. *MOL CELL* **74** 640 (2019).
- <sup>2</sup> Knuckles, P. *et al.*, RNA fate determination through cotranscriptional adenosine methylation and microprocessor binding. *NAT STRUCT MOL BIOL* **24** 561 (2017).
- <sup>3</sup> Barbieri, I. *et al.*, Promoter-bound METTL3 maintains myeloid leukaemia by m(6)A-dependent translation control. *NATURE* **552** 126 (2017).
- <sup>4</sup> Xiao, S. *et al.*, The RNA N(6)-methyladenosine modification landscape of human fetal tissues. *NAT CELL BIOL* **21** 651 (2019).
- <sup>5</sup> Garcia-Perez, J. L., Widmann, T. J. & Adams, I. R., The impact of transposable elements on mammalian development. *DEVELOPMENT* **143** 4101 (2016).
- <sup>6</sup> Allshire, R. C. & Madhani, H. D., Ten principles of heterochromatin formation and function. *Nat Rev Mol Cell Biol* **19** 229 (2018).
- <sup>7</sup> Rowe, H. M. & Trono, D., Dynamic control of endogenous retroviruses during development. *VIROLOGY* **411** 273 (2011).
- <sup>8</sup> Matsui, T. *et al.*, Proviral silencing in embryonic stem cells requires the histone methyltransferase ESET. *NATURE* **464** 927 (2010).
- <sup>9</sup> Rowe, H. M. *et al.*, KAP1 controls endogenous retroviruses in embryonic stem cells. *NATURE* **463** 237 (2010).
- <sup>10</sup> Schotta, G. *et al.*, A silencing pathway to induce H3-K9 and H4-K20 trimethylation at constitutive heterochromatin. *Genes Dev* **18** 1251 (2004).
- <sup>11</sup> Bujnicki, J. M., Feder, M., Radlinska, M. & Blumenthal, R. M., Structure prediction and phylogenetic analysis of a functionally diverse family of proteins homologous to the MT-A70 subunit of the human mRNA: m(6) a methyltransferase. *J MOL EVOL* **55** 431 (2002).
- <sup>12</sup> Zheng, G. *et al.*, ALKBH5 is a mammalian RNA demethylase that impacts RNA metabolism and mouse fertility. *MOL CELL* **49** 18 (2013).
- <sup>13</sup> Elsasser, S. J., Noh, K. M., Diaz, N., Allis, C. D. & Banaszynski, L. A., Histone H3.3 is required for endogenous retroviral element silencing in embryonic stem cells. *NATURE* **522** 240 (2015).
- <sup>14</sup> Walsh, C. P., Chaillet, J. R. & Bestor, T. H., Transcription of IAP endogenous retroviruses is constrained by cytosine methylation. *NAT GENET* **20** 116 (1998).

- <sup>15</sup> Wang, X. *et al.*, N6-methyladenosine-dependent regulation of messenger RNA stability. *NATURE* **505** 117 (2014).
- <sup>16</sup> Lasman, L. *et al.*, Context-dependent functional compensation between Ythdf m(6)A reader proteins. *Genes Dev* **34** 1373 (2020).
- <sup>17</sup> Zaccara, S. & Jaffrey, S. R., A Unified Model for the Function of YTHDF Proteins in Regulating m(6)A-Modified mRNA. *CELL* **181** 1582 (2020).
- <sup>18</sup> Wang, P., Doxtader, K. A. & Nam, Y., Structural Basis for Cooperative Function of Mettl3 and Mettl14 Methyltransferases. *MOL CELL* **63** 306 (2016).
- <sup>19</sup> Yue, Y. *et al.*, VIRMA mediates preferential m(6)A mRNA methylation in 3'UTR and near stop codon and associates with alternative polyadenylation. *CELL DISCOV* **4** 10 (2018).
- <sup>20</sup> Li, X. *et al.*, GRID-seq reveals the global RNA-chromatin interactome. *NAT BIOTECHNOL* **35** 940 (2017).
- <sup>21</sup> Dominissini, D. *et al.*, Topology of the human and mouse m6A RNA methylomes revealed by m6A-seq. *NATURE* **485** 201 (2012).
- <sup>22</sup> Meyer, K. D. *et al.*, Comprehensive Analysis of mRNA Methylation Reveals Enrichment in 3' UTRs and near Stop Codons. *CELL* **149** 1635 (2012).
- <sup>23</sup> Xiao, Y. *et al.*, An Elongation- and Ligation-Based qPCR Amplification Method for the Radiolabeling-Free Detection of Locus-Specific N(6) -Methyladenosine Modification. *Angew Chem Int Ed Engl* **57** 15995 (2018).
- <sup>24</sup> Xu, C. *et al.*, Structural basis for selective binding of m6A RNA by the YTHDC1 YTH domain. *NAT CHEM BIOL* **10** 927 (2014).
- <sup>25</sup> Patil, D. P. *et al.*, m(6)A RNA methylation promotes XIST-mediated transcriptional repression. *NATURE* **537** 369 (2016).
- <sup>26</sup> Martienssen, R. & Moazed, D., RNAi and heterochromatin assembly. *Cold Spring Harb Perspect Biol* **7** a19323 (2015).
- <sup>27</sup> Berrens, R. V. *et al.*, An endosiRNA-Based Repression Mechanism Counteracts Transposon Activation during Global DNA Demethylation in Embryonic Stem Cells. *CELL STEM CELL* **21** 694 (2017).
- <sup>28</sup> Zofall, M. *et al.*, RNA Elimination Machinery Targeting Meiotic mRNAs Promotes Facultative Heterochromatin Formation. *SCIENCE* **335** 96 (2012).
- <sup>29</sup> Wang, C. *et al.*, A novel RNA-binding mode of the YTH domain reveals the mechanism for recognition of determinant of selective removal by Mmi1. *NUCLEIC ACIDS RES* **44** 969 (2016).
- <sup>30</sup> Harigaya, Y. *et al.*, Selective elimination of messenger RNA prevents an incidence of untimely meiosis. *NATURE* **442** 45 (2006).

**Fig. 1. METTL3 binds endogenous retroviral elements**

a: Bar graph showing the overlapping ratios (Jaccard statistics, see Methods) of METTL3 peaks with peaks of different histone modifications.

b: Heatmaps showing ChIP-seq enrichments ( $\log_2(\text{ChIP}/\text{Input})$ ) of METTL3, H3K9me3 and H4K20me3 on METTL3 peaks.

c: Heatmap showing co-enrichment of METTL3, H3K9me3 and H4K20me3 on the ERVK subclasses. The 5 most and 5 least METTL3-enriched ERVK subclasses are displayed.

d-e: Scatter plots showing the correlation between METTL3 and H3K9me3 (d) or H4K20me3 (e) on IAPez-int ( $n=2,542$ ).  $p$  value =  $1.7\text{e-}177$  (d) and  $2.4\text{e-}151$  (e), two-sided Pearson's correlation test.

f: UCSC genome browser snapshots showing the binding pattern of METTL3, histone modifications and input on representative IAPez elements.

Uniquely mapped ChIP-seq reads were used in panel a, b, d, e, f. Uniquely+randomly mapped ChIP-seq reads were used in panel c.

Heatmaps were ranked according to METTL3 enrichment in parental cells in descending order in panel b.

**Fig. 2. METTL3 is required for heterochromatin formation over repetitive elements**

a-b: Heatmaps (a) and UCSC genome browser snapshot (b) showing binding patterns of H3K9me3 (Left) and H4K20me3 (Right) on IAPeZ-int elements in parental, *Mettl3* KO and rescued cell lines with METTL3<sup>WT</sup> or METTL3<sup>APPA</sup>.

c: Boxplot showing RNA levels of the IAPeZ-int (n=2,542) in parental, *Mettl3* KO and rescued cell lines with METTL3<sup>WT</sup> or METTL3<sup>APPA</sup>. \*\*\*\*  $p < 0.0001$  (Exact  $p$  values from left to right: 4.4e-273, 1.1e-286, 0), two-sided paired t-test.

d: RT-qPCR showing relative expression levels of IAPeZ-int (Left) and *Nxt1* (Right) in parental and *Mettl3* KO cell lines treated with Actinomycin D at different time points. Relative RNA levels (normalized to *Actin*) are normalized to t=0. The mean of three biological replicates  $\pm$  s.d. is shown. \* $p < 0.05$ , \*\* $p < 0.01$ , two-sided t-test. Exact  $p$  values are provided in the Source Data.

Uniquely mapped ChIP-seq and RNA-seq reads were used in panel a, b, c.

Heatmaps were ranked according to METTL3 density in parental cells in descending order in panel a.

For boxplot in panel c, the middle line, lower and upper hinge of the boxplot correspond to the median, the first and third quartiles, respectively. The whiskers extend from the hinges to no further than  $1.5 \times \text{IQR}$  (inter-quartile range) from the hinge. Outlying points that are plotted individually.

**Figure 3. METTL3 regulates SETDB1/TRIM28 localization to IAPEz elements**

a-b: Heatmaps (a), and UCSC genome browser snapshot (b) showing binding patterns of METTL3 on IAPEz-int elements in parental, *Mettl3* KO and rescued cell lines with METTL3<sup>WT</sup> or METTL3<sup>APPA</sup>.

c: Western blots showing reciprocal immunoprecipitation of METTL3, SETDB1 and TRIM28.

d: Heatmaps showing binding patterns of SETDB1 (Left) and TRIM28 (Right) on IAPEz-int elements in parental and *Mettl3* KO cells.

e: UCSC genome browser snapshot showing binding patterns of SETDB1 (Upper) TRIM28 (Lower) on IAPEz-int elements in parental and *Mettl3* KO cells.

Uniquely mapped ChIP-seq reads were used in panel a, b, d, e.

Heatmaps were ranked according to METTL3 density in parental cells in descending order (a, d).

For blots, representative of two independent experiments in panel c. For blots source data, see Supplementary Figure 1.

**Fig. 4. YTHDC1 recruited by METTL3 dependent m<sup>6</sup>A contributes to METTL3 binding and heterochromatin formation on IAPEz-int**

a: Aggregation plot showing the average enrichment of m<sup>6</sup>A and input over IAPEz-int in parental cell line.

b: Aggregation plot showing the average enrichment levels of m<sup>6</sup>A ( $\log_2(\text{m}^6\text{A}/\text{input})$ ) over IAPEz-int in parental and *Mettl3* KO cell lines.

c: Aggregation plot showing the average enrichment of m<sup>6</sup>A and input over IAPEz-int in *Setdb1* CKO cell line.

d: qPCR showing SELECT results for detecting listed Adenosine positions in IAPEz-int consensus sequence in parental and *Mettl3* KO cells. The mean of three biological replicates  $\pm$  s.d. is shown. \*  $p < 0.05$ , \*\*  $p < 0.01$ , two-sided t-test. Exact  $p$  values are provided in the Source Data.

e: Heatmaps showing YTHDC1 enrichment on the IAPEz-int elements in parental, *Mettl3* KO and rescued cell lines with METTL3<sup>WT</sup> or METTL3<sup>APPA</sup>.

f-g: Heatmaps showing METTL3 (f) and H3K9me3 (g) enrichment on the IAPEz-int elements in YTHDC1<sup>WT</sup>, *Ythdc1* KO and YTHDC1<sup>W429A</sup> cell lines.

h: Boxplot showing RNA levels on the IAPEz-int elements ( $n=2,542$ ) in YTHDC1<sup>WT</sup>, *Ythdc1* KO and YTHDC1<sup>W429A</sup> cell lines. \*\*\*\*  $p < 0.0001$  (Exact  $p$  values from left to right:  $2.4 \times 10^{-78}$ ,  $7.0 \times 10^{-143}$ ), two-sided paired t-test.

i: Western blots showing reciprocal immunoprecipitation of METTL3 and YTHDC1.

Uniquely mapped reads were used in panel a, b, c, e, f, g, h.

Heatmaps were ranked according to METTL3 density in parental cells in descending order in panel e, f, g.

For boxplot in panel h, the middle line, lower and upper hinge of the boxplot correspond to the median, the first and third quartiles, respectively. The whiskers extend from the hinges to no further than  $1.5 \times \text{IQR}$  (inter-quartile range) from the hinge. Outlying points that are plotted individually.

For blots, representative of two independent experiments in panel i. For blots source data, see Supplementary Figure 1.

## Methods

### Antibodies

METTL3 (Bethyl, #A301-567A, 1/3000 for WB), METTL3 (Abcam, #ab195352, only used in Extended Data Fig. 1h), METTL3 (Proteintech, #15073-1-AP, only used in Extended Data Fig. 1h), TRIM28 (Bethyl, #A300-274A, 1/2000 for WB), SETDB1 (Proteintech, #11231-1-AP, 1/2000 for WB), H3K9me3 (Active Motif, #39161), H4K20me3 (Abcam, #ab9053), H3K4me3 (CST, #9751), H3K27me3 (CST, #9733), H3.3 (Millipore, #09-838), Cas9 (Active motif, #61757, 1/1000 for WB), m<sup>6</sup>A (Synaptic Systems, #202003), YTHDC1 (CST, #77422, 1/2000 for WB), RBM15 (Proteintech, #10587-1-AP, 1/2000 for WB), RBM15B (Proteintech, #22249-1-AP, 1/2000 for WB), METTL14 (Sigma, #HPA038002, 1/2000 for WB), WTAP (Proteintech, #10200-1-AP, 1/2000 for WB), ZC3H13 (Bethyl, #A300-748A, 1/2000 for WB), Virilizer (Bethyl, #A302-124A, 1/2000 for WB), ALKBH5 (#ab195377, 1/1000 for WB), HNRNPA2B1 (Proteintech, #14813-1-AP), HNRNPC (Proteintech, #11760-1-AP), HNRNPK (Proteintech, #11426-1-AP).

### mES cell culture

E14Tg2a murine embryonic stem cells (mESCs, gift from Qi-Long Ying, USC) were cultured in Dulbecco's Modified Eagle's Medium (DMEM) supplemented with 10% fetal FBS (Gibco, #16000-044), 1% MEM non-essential amino acid (Gibco, #11140), 55 mM β-Mercaptoethanol (Gibco, #21985-023), 100 U/mL Penicillin/Streptomycin (Hyclone, #SV30010), 1000 units/mL LIF (Millipore, #ESG1107) and MEK inhibitor PD0325901 (1 μM) and GSK3β

inhibitor CH99021 (3  $\mu$ M) at 37°C with 5% CO<sub>2</sub>.

For EB differentiation, embryoid bodies (EBs) were allowed to form in the absence of LIF by hanging drops containing 1,000 mES cells/drop on petri dish lids for 2 days, and then collected and transferred to standard mES culture (without LIF and MEK and GSK3 $\beta$  inhibitor) in non-coated petri dishes 5 days.

#### **ChIP-qPCR and ChIP-seq**

ChIP assays were performed as described elsewhere<sup>31</sup>. Briefly, chromatin samples were incubated with specific antibodies in the ChIP lysis buffer (20 mM Tris-HCl pH 8.1, 150 mM NaCl, 2 mM EDTA, 1% TritonX-100 and 0.05% SDS) overnight at 4°C. The protein-DNA complexes were immobilized on pre-washed protein A/G beads. The bound fractions were washed 3 times with the Lysis buffer, and twice with the Low Salt Wash buffer (10 mM Tris-HCl, 250 mM LiCl, 1 mM EDTA, 0.5% NP-40, 0.5% Na-deoxycholate), and once with 10 mM Tris-HCl pH 8.0. Elution and reverse crosslinking were carried out in the Elution buffer (50 mM Tris-HCl pH 8.0, and 1% SDS) at 65°C for 5 hours. After 1 hour of RNase A (1 unit/ $\mu$ l) at 37°C and Proteinase K (1 unit/ $\mu$ l) digestion at 55°C, DNA samples were then purified using PCR extraction kit (QIAGEN, #28006). The precipitated DNA samples were either analyzed by qPCR (primer sequences are listed in Supplementary Table 1) or prepared for DNA deep sequencing according to manufacturer's guidelines (SWIFT, #21096).

## RT-qPCR

Total RNAs from mESCs were isolated using TRIzol reagent (Invitrogen, #15596018) and treated with TURBO™ DNase using TURBO DNA-free Kit (Invitrogen, #AM1970) according to the manufacturer's instruction. cDNAs were synthesized with PrimeScript RT reagent kit (Takara, #RR037A) containing random primers using 1µg of RNA per sample. RT-qPCR was performed using SYBR Premix ExTaq (Takara, #RR420Q) with the Roche Lightcycler 480 Instrument II system. Primer sequences are listed in Supplementary Table 1.

Subcellular fractions were collected as following: mESCs were washed once with PBS and lysed in buffer A (10 mM HEPES pH 7.5, 1.5 mM MgCl<sub>2</sub>, 10 mM KCl, 0.5 mM DTT, 1 mM PMSF and 1x Protease Inhibitor Cocktail) on ice for 15 min, then NP-40 was added to a final concentration of 0.25% for another 5 min. Nuclei were collected by centrifugation (2,000 rpm, 3 min, 4°C) with the supernatant as cytoplasmic fraction. The nuclei were re-suspended in buffer C (20 mM HEPES, pH 7.5, 10% Glycerol, 0.42 M KCl, 4 mM MgCl<sub>2</sub>, 0.2 mM EDTA, 0.5 mM DTT, 1 mM PMSF and 1x Protease Inhibitor Cocktail). After 30 min incubation on ice, nuclear extract was collected by high speed centrifugation (13,000 rpm, 15 min, 4°C) as nuclear fraction. Insoluble chromatin fraction was re-suspended with buffer A. RNAs in different subcellular fractions were isolated using TRIzol reagent (Invitrogen, #15596018) and treated with TURBO™ DNase using TURBO DNA-free Kit (Invitrogen, #AM1970) according to the manufacturer's instruction.

## Construction of stable cell lines and knockdown

CRISPR-Cas9 gene targeting was carried out as previously described<sup>32</sup> and the single knockout clones were isolated and then confirmed by Western blot showing undetectable protein. *Mettl3*, *Mettl14* and *Alkbh5* KO cells were created by introduction of one sgRNA. *Rbm15/15b* double KO cells were created by simultaneous introduction of two sgRNAs targeting *Rbm15*, and two sgRNAs targeting *Rbm15b*. Guiding RNA sequences and donor sequence used are listed in Supplementary Table 2.

*Setdb1* CKO mESCs were kindly provided by Yoichi Shinkai (REKIN). *Setdb1* CKO mESCs carried one null and one floxed allele of *Setdb1*, which could be deleted upon CRE-mediated excision. Treatment with 4-hydroxytamoxifen (4-OHT) induced the activation of ligand binding domain of estrogen receptor and CRE recombinase fusion protein, leading to conditional deletion of the remaining allele<sup>8</sup>. For 4-OHT treatment, mESCs were cultured in ES medium with 800 nM 4-OHT for 4 days, and further cultured without 4-OHT for 2 days. Depletion of SETDB1 was validated by Western blotting.

For rescued cells, cDNA of full-length murine METTL3 WT (NCBI RefSeq: NM\_019721.2) or METTL3 mutation (DPPW motif to APPA, W475A, N477A) were cloned into the pPB-CAG-IRES-Pac plasmid (Puromycine resistant). These plasmids were individually co-transfected into mESCs with pCMV-PBase plasmid in a 1:1 ratio using Lipofectamine 2000 (Invitrogen, #11668-019) according to the manufacturer's instruction. Medium was replaced

by fresh media with 2 µg/mL Puromycine after 48 hours post-transfection. After continuous selection for 5 days, the surviving mESCs were pooled as stable rescued cell lines.

Construction of YTHDC1<sup>WT</sup>, *Ythdc1* KO, and YTHDC1<sup>W429A</sup> mESCs in auxin-inducible degron (AID) system is shown in Extended Data Fig. 7f. Briefly, AID-tag-fused YTHDC1 (NCBI Reference Sequence: NM\_177680.4, resistant to gRNA, c.1264\_1290CATGGCGGATCTCCTATACAC>CACGGAGGCAGCCCCATCCAT) was cloned into the pPB-CAG-IRES-Pac plasmid (Puromycine resistant), and TIR1 was cloned into the pPB-CAG-IRES-Pac plasmid (Blasticidin S resistant). mESCs were randomly integrating the expression cassettes expressing TIR1 and AID-tag-fused YTHDC1 into the genome, followed by knocking out the endogenous *Ythdc1* with gRNA, or knocking in the YTHDC1<sup>W429A</sup> mutation into the endogenous *Ythdc1* with gRNA and donor. Single colonies were picked and positive colonies were identified by PCR genotyping.

For the dCas9 experiment in Extended Data Fig. 4l-n and 8m-n, the gRNA expression plasmids were cloned by inserting annealed oligos into the modified pgRNA plasmid (Addgene plasmid: 44248). The PiaggyBac-dCas9-METTL3<sup>WT</sup>/METTL3<sup>APPA</sup> or YTHDC1 were cloned by replacing the DNMT3A fragment (138-dCas9-DNMT3A, addgene plasmid: 84570)<sup>33</sup>. Lentiviruses expressing gRNAs were produced by co-transfection of gRNA plasmids (Ctrl. or 5 different IAP 5'UTR gRNAs mixed equally, sequences are listed in Supplementary Table 2) with VSV-G and psPAX2 in a 3:1:1 ratio into HEK293T cells. Supernatant at 48 hours post-

transfection was collected. *Mettl3* KO mESCs were seeded in a 6-well plate and infected with each gRNA lentivirus supernatant in the presence of 5 µg/mL polybrene. Medium was replaced by fresh media with Puromycine (2 µg/ml) for 5 days, the surviving mESCs were pooled as stably infected mESCs. To generate stable cell lines with integrated Doxycycline-inducible transgenes for dCas9-METTL3 or dCas9-YTHDC1, the dCas9-METTL3 or dCas9-YTHDC1 plasmids were co-transfected into mESCs expressing gRNA with pCMV-PBase plasmid and selected with G418 (400 µg/ml) for 10 days. Doxycycline was added to the cell culture media to a final concentration of 2 µg/mL for 5 days for ChIP experiments.

For the dCas9 experiment in Extended Data Fig. 8o-p, the *Mettl3* KO+METTL3<sup>APPA</sup> stable cell line (Blasticidin S resistant) was first generated. METTL3<sup>APPA</sup> mutation was cloned into the pPB-CAG-IRES-Pac plasmid (Blasticidin S resistant). This plasmid was co-transfected into mESCs with pCMV-PBase plasmid in a 1:1 ratio using Lipofectamine 2000 (Invitrogen, #11668-019) according to the manufacturer's instruction. Medium was replaced by fresh media with 10µg/mL Blasticidin S 48 hours post-transfection. After continuous selection for 7 days, the surviving mESCs were pooled as stable rescued cell lines. *Mettl3* KO+METTL3<sup>APPA</sup> mESCs were seeded in a 6-well plate and infected with gRNA lentivirus in the presence of 5 µg/mL polybrene. Medium was replaced by fresh media with Puromycine (2 µg/ml) for 5 days, the surviving mESCs were pooled as stably infected mESCs. To generate stable cell lines with integrated Doxycycline-inducible transgenes for dCas9-YTHDC1, YTHDC1 plasmid was co-transfected into mESCs expressing gRNA with pCMV-PBase plasmid and selected with G418 (400 µg/ml) for 10 days. Doxycycline was added to the cell culture media to a final

concentration of 2 µg/mL for 5 days for ChIP experiments.

SiRNA-mediated gene knockdown was performed using Lipofectamine RNAiMAX (Invitrogen, #13778-150) with siRNA at 25 nM final concentration. Cells were harvested after 3 days. SiRNA oligonucleotides are listed at Supplementary Table 3.

### **Isolation of mRNA for QQQ and HPLC analysis**

mRNA was isolated from 1 µg total RNA with Oligo d(T)<sub>25</sub> magnetic beads (NEB, #S1419S), followed with RiboMinus Kit (Invitrogen, #A15026). Purified mRNA was digested by nuclease P1 (Thermo, #18009027) in 25 µl of buffer containing 25 mM NaCl and 2.5 mM of ZnCl<sub>2</sub> at 42°C for 2 hours, which was followed by addition of NH<sub>4</sub>HCO<sub>3</sub> (1 M, 3 µl) and alkaline phosphatase (Sigma, #P4252) and additional incubation at 37°C for 2 hours. Samples were then diluted to 60 µl and 5 µl of solution was loaded into liquid chromatography-tandem mass spectrometry (LC-MS/MS) (Agilent 6410 QQQ Triple-Quadrupole Mass Spectrometer).

### **The SELECT detection assay**

SELECT (single base elongation- and ligation-based qPCR amplification method) was carried out as previously described<sup>23</sup>. Briefly, 1 µg total RNA was mixed with 40 nM Up Primer, 40 nM Down Primer and 5 µM dNTP in 17 µl 1×CutSmart buffer (NEB, #B7204S). The RNA and primers were annealed by incubating mixture at a temperature gradient: 90°C for 1 min, 80°C

for 1 min, 70°C for 1 min, 60°C for 1min, 50°C for 1 min, and then 40°C for 6 min. Subsequently, a 3 µl of mixture containing 0.01 U Bst 2.0 DNA polymerase, 0.5 U SplintR ligase and 10 nmol ATP was added in the former mixture to the final volume 20 µl. The final reaction mixture was incubated at 40°C for 20 min, denatured at 80°C for 20 min. The qPCR reaction was performed using SYBR Premix Ex Taq (Takara, #RR420Q) with the Roche Lightcycler 480 Instrument II system. IAPez-int consensus sequence was downloaded from Repbase. Primer sequences are listed in Supplementary Table 4.

#### **In vitro m<sup>6</sup>A methylation assay**

The in vitro m<sup>6</sup>A methylation assay was carried out in a 20µl reaction mixture containing 0.5µg METTL3/METTL14 protein (Active motif, #31970), 0.5µg RNA oligonucleotides, 20 mM Tris (pH 7.5), 0.01% Triton-X, 1 mM DTT, 50 mM ZnCl<sub>2</sub>, 0.2 U/mL RNasin, 1% glycerol, and 460 nM [<sup>3</sup>H]-SAM. Each in vitro m<sup>6</sup>A methylation reaction was incubated at room temperature for 1 hour. RNA was extract with Trizol and dissolved in 20µl H<sub>2</sub>O. The counts per minute (C.P.M.) of the RNA was measured in a scintillation counter.

#### **WGBS library preparation**

The bisulfate conversion was performed using the EZ DNA Methylation Gold kit from Zymo Research (#D5005). Post-BS library preparation was performed using Accel-NGS Methyl-Seq DNA Library Kit from Swift Biosciences (SWIFT, #36024).

### **Strand specific total RNA-seq**

Specific total RNA library preparation was performed using NEBNext Ultra Directional RNA Library Prep Kit for Illumina (NEB, #E7420S).

### **ChIRP-seq**

ChIRP was performed according to the previous work with some modifications<sup>34</sup>. mESCs were crosslinked with 3% formaldehyde for 30 min at room temperature. Crosslinking was then quenched with 0.125 M glycine for 5 min. Chromatin was then solubilized by sonicating in lysis buffer (50 mM Tris 7.0, 10 mM EDTA, 1% SDS, 0.5 mM DTT, and RNase Inhibitors). Chromatin is diluted in two times volume of hybridization buffer (750 mM NaCl, 1% SDS, 50 mM Tris 7.0, 1 mM EDTA, 15% Formamide, 0.5 mM DTT, and RNase Inhibitors). 10 pmol probes (20 probes mixed equally, sequences are listed in Supplementary Table 5) were added to diluted chromatin, which was mixed by end-to-end rotation at 37°C for 6 hours, followed by the addition of Streptavidin beads for another 45 min at 37°C. The bound fractions were washed 5 times with wash buffer (2x SSC, 0.5% SDS, add DTT and RNase Inhibitors). Elution and reverse crosslinking were carried out at 65°C overnight. After 1 hour of RNase A (1unit/μl) at 37°C and Proteinase K (1 unit/μl) digestion at 55°C, DNA samples were then purified using PCR extraction kit (QIAGEN, #28006). The precipitated DNA samples were prepared for DNA deep sequencing according to manufacturer's guidelines (SWIFT, #21096).

### **Flavopiridol, Triptolide, $\alpha$ -Amanitin or Actinomycin D treatment**

For transcription inhibition<sup>35</sup>, mESCs were treated with 1 $\mu$ M Flavopiridol, or 1 $\mu$ M Triptolide added directly to the culture media and cells were incubated with the drug for 12 hours at 37°C, or 10 $\mu$ M  $\alpha$ -Amanitin for 24 hours at 37°C for ChIP experiments. mESCs were treated with 2.5  $\mu$ g/ml Actinomycin D directly to the culture media and cells were incubated with the drug for different time points (1, 3, 5, 7, 10 hours) at 37°C for the RNA decay experiments.

### **Co-Immunoprecipitation**

mESCs were washed once with PBS and lysed in buffer A (10 mM HEPES pH 7.5, 1.5 mM MgCl<sub>2</sub>, 10 mM KCl, 0.5 mM DTT, 10 mM Nethylmaleimide (NEM), 1mM PMSF and 1x Protease Inhibitor Cocktail) on ice for 15 min, then NP-40 was added to a final concentration of 0.25% for another 5 min. Nuclei were collected by centrifugation (2,000 rpm, 3 min, 4°C) and re-suspended in buffer C (20 mM HEPES, pH 7.5, 10% Glycerol, 0.42 M KCl, 4 mM MgCl<sub>2</sub>, 0.2 mM EDTA, 0.5 mM DTT, 10 mM Nethylmaleimide (NEM), 1 mM PMSF and Protease Inhibitor Cocktail). After 30 min incubation on ice, nuclear extract was collected by high speed centrifugation (13,000 rpm, 15 min, 4°C) as nuclear extract A. Insoluble chromatin fraction was re-suspended with buffer A (2X volumes of buffer C) with DNase I. After 30 min incubation at 37°C, the soluble fraction was collected by high speed centrifugation (13,000 rpm, 15 min, 4°C) as nuclear extract B. Nuclear extract A and nuclear extract B were mixed and incubated with indicated antibody or IgG for 6 hours at 4°C, followed by the addition of Dynabeads protein A/G for another 2 hours. The beads were washed for 4 times with wash

buffer (Mixture of buffer A and buffer C in a ratio of 2:1). SDS buffer was directly added to the beads and boiled for 10 min. The samples were loaded on SDS-PAGE gels and subjected to immunoblotting using indicated antibodies.

### **MeRIP-seq**

For chromatin RNA MeRIP-seq, chromatin RNA was collected as described above. 20 µg RNA was sonicated to 100-200nt fragments by Bioruptor Plus sonicator device (Diagenode) and incubated with 5µg anti-m<sup>6</sup>A antibody in 1 x IP buffer (10 mM Tris-HCl, pH 7.4, 150 mM NaCl, 0.1% NP-40) for 2 hours at 4°C. The m<sup>6</sup>A-IP mixture was then incubated with Dynabeads protein A/G for an additional 2 hours at 4°C on a rotating wheel. After washing 3 times with 1 x IP buffer, the bound RNA was isolated with TRIzol reagent. The purified RNA fragments from MeRIP and Input RNA were first treated with Ribo-off rRNA Depletion Kit (Vazyme, #N406), followed with library construction using NEBNext Ultra Directional RNA Library Prep Kit for Illumina (NEB, #E7420) according to manufacturer's guidelines.

### **ChIP-seq analysis**

Raw reads were trimmed using Trim\_galore (v0.6.4\_dev) and aligned to the mm10 genome using Bowtie2 (v2.2.5)<sup>36</sup> to report best alignment with MAPQ. Unique reads were filtered by MAPQ>20. PCR duplicates were removed using samtools (v1.7)<sup>37</sup> rmdup. Genome coverage bedGraph files for UCSC genome browser were generated by deeptools (v3.0.2)<sup>38</sup> bamCoverage with the parameters “-of bedgraph --normalizeUsing RPKM --binSize 5”. Peaks

were generated by macs2 (2.1.4)<sup>39</sup> callpeak with parameters “-p 0.00001 --nomodel”. Peak annotation was carried out using Homer (v4.8.2)<sup>40</sup> annotatePeaks.pl. The Jaccard statistic representing the ratio of the intersection of two sets to the union of the two sets is calculated using bedtools (v2.29.2)<sup>41</sup>. The relative distances between each interval in one set and the two closest intervals in another set is calculated using bedtools (v2.29.2)<sup>41</sup>. Genome coverage bigwig files for heatmap and aggregation plot were generated by deeptools (v3.0.2)<sup>38</sup> bamCoverage with the parameter “--normalizeUsing RPKM --binSize 5”. Heatmaps were generated by deeptools (v3.0.2)<sup>38</sup> computeMatrix and plotHeatmap. Aggregation plots were generated by deeptools (v3.0.2)<sup>38</sup> computeMatrix and plotProfile. ChIP-seq density on repetitive elements were calculated by Homer (v4.8.2)<sup>40</sup> analyzeRepeats.pl. Boxplot were generated by R boxplot. METTL3 peak is listed in Supplementary Table 6.

## **WGBS analysis**

Raw reads were trimmed 10 bps off at the 5’ end and 3’ end and then mapped to mm10 genome using bsmmap (v2.90)<sup>42</sup> with the parameters “-p 10 -w 50 -v 0.1”. Methylation ratios were calculated by methratio.py with the parameters “-t 2 -m 5 -z”. Methylation over a given genomic feature was calculated by averaging the individual methylation levels of CpGs and only features with at least 10 covered CpGs were used. Boxplot were generated by R boxplot.

## **Total RNA-seq analysis**

Raw reads were trimmed using Trim\_galore (v0.6.4\_dev) and aligned to the mm10 genome

using TopHat (v2.1.1)<sup>43</sup> with parameter “--max-multihits 1”. PCR duplicates were removed using samtools (v1.7)<sup>37</sup> rmdup. Strand specific reads were separated by samtools (v1.7)<sup>37</sup> view with specific flags 99, 147, 83, 163. Strand specific density on repetitive elements were calculated by Homer (v4.8.2)<sup>40</sup> analyzeRepeats.pl with the parameter “strand”. Boxplot were generated by R boxplot.

### **ChIRP-seq analysis**

Raw reads were trimmed using Trim\_galore (v0.6.4\_dev) and aligned to the mm10 genome using Bowtie2 (v2.2.5)<sup>36</sup> to report best alignment with MAPQ. PCR duplicates were removed using samtools (v1.7)<sup>37</sup> rmdup. Genome coverage bigwig files aggregation plot were generated by deeptools (v3.0.2)<sup>38</sup> bamCoverage with the parameter “--normalizeUsing RPKM --binSize 5”. Aggregation plots were generated by deeptools (v3.0.2)<sup>38</sup> computeMatrix and plotProfile.

### **MeRIP-seq analysis**

Raw reads were trimmed using Trim\_galore (v0.6.4\_dev) and aligned to the mm10 genome using TopHat (v2.1.1) with parameter “--max-multihits 1”. PCR duplicates were removed using samtools<sup>37</sup> (v1.7) rmdup. Strand specific reads were separated by samtools<sup>37</sup> (v1.7) view with specific flags 99, 147, 83, 163. Genome coverage bedGraph files for UCSC genome browser were generated by deeptools (v3.0.2)<sup>38</sup> bamCoverage with the parameters “- of bedgraph --normalizeUsing RPKM --binSize 5”. m<sup>6</sup>A/Input ratio bigwig files for aggregation plot were generated by deeptools (v3.0.2)<sup>38</sup> bamCompare with the parameter “--

normalizeUsing RPKM --binSize 5". Aggregation plots were generated by deeptools (v3.0.2)<sup>38</sup> computeMatrix and plotProfile. m<sup>6</sup>A peak calling was performed using a "sliding window" method slightly modified from the previous study<sup>22</sup>. Briefly, reads numbers of IP and Input were calculated on every 25bp window across genome. Windows with normalized IP/Input density  $\geq 2$ , Fisher's Exact Test p-value  $<0.05$  were selected. Adjacent windows were merged using bedtools (v2.29.2)<sup>41</sup> and the merged regions with size  $\geq 100$ bp were determined as m<sup>6</sup>A peak. Consensus motifs are called using Homer (v4.8.2)<sup>40</sup> findMotifsGenome.pl with the parameter "-rna".

- <sup>31</sup> Lan, F. *et al.*, A histone H3 lysine 27 demethylase regulates animal posterior development. *NATURE* **449** 689 (2007).
- <sup>32</sup> Maeder, M. L. *et al.*, CRISPR RNA-guided activation of endogenous human genes. *NAT METHODS* **10** 977 (2013).
- <sup>33</sup> Liu, X. S. *et al.*, Editing DNA Methylation in the Mammalian Genome. *CELL* **167** 233 (2016).
- <sup>34</sup> Chu, C., Qu, K., Zhong, F. L., Artandi, S. E. & Chang, H. Y., Genomic maps of long noncoding RNA occupancy reveal principles of RNA-chromatin interactions. *MOL CELL* **44** 667 (2011).
- <sup>35</sup> Bensaude, O., Inhibiting eukaryotic transcription: Which compound to choose? How to evaluate its activity? *Transcription* **2** 103 (2011).
- <sup>36</sup> Langmead, B. & Salzberg, S. L., Fast gapped-read alignment with Bowtie 2. *NAT METHODS* **9** 357 (2012).
- <sup>37</sup> Li, H. *et al.*, The Sequence Alignment/Map format and SAMtools. *BIOINFORMATICS* **25** 2078 (2009).
- <sup>38</sup> Ramirez, F. *et al.*, deepTools2: a next generation web server for deep-sequencing data analysis. *NUCLEIC ACIDS RES* **44** W160 (2016).
- <sup>39</sup> Zhang, Y. *et al.*, Model-based analysis of ChIP-Seq (MACS). *GENOME BIOL* **9** R137 (2008).
- <sup>40</sup> Heinz, S. *et al.*, Simple combinations of lineage-determining transcription factors prime cis-regulatory elements required for macrophage and B cell identities. *MOL CELL* **38** 576 (2010).
- <sup>41</sup> Quinlan, A. R. & Hall, I. M., BEDTools: a flexible suite of utilities for comparing genomic features. *BIOINFORMATICS* **26** 841 (2010).
- <sup>42</sup> Xi, Y. & Li, W., BSMAP: whole genome bisulfite sequence MAPping program. *BMC*

728 *BIOINFORMATICS* **10** 232 (2009).

729 <sup>43</sup> Trapnell, C., Pachter, L. & Salzberg, S. L., TopHat: discovering splice junctions with  
730 RNA-Seq. *BIOINFORMATICS* **25** 1105 (2009).

731

732

## Acknowledgements

We thank Danesh Moazed (Harvard Medical School) and Erdem Sendinc (Boston Children's Hospital) for critical reading of the manuscript and suggestions. We thank Jiekai Chen (Guangzhou Institutes of Biomedicine and Health, Chinese Academy of Sciences) for suggestions and for sharing unpublished results. We thank Yoichi Shinkai (REKIN) for sharing the *Setdb1* CKO cell line. H.S. was supported by Shanghai Rising-Star Program (19QA1401300) and National Science Foundation of China (81874157, 32070649, 31601060). W.X. was supported by National Science Foundation of China (31900469). Y.S. is an American Cancer Society Research Professor.

## Author contributions

W.X. and H.S. carried out most of the experiments and bioinformatics analyses described in this manuscript. J.L. carried out YTHDC1<sup>W429A</sup> identification and genotyping. C.H. carried out LC-MS/MS analysis of m<sup>6</sup>A. J.W. and J.D. provided discussions and advice on co-immunoprecipitation. L.T. provided discussions and advice on mES cell culture. L.W., J.W. and B.R. provided discussions and advice on ChIP. H.M. and F.W. provided discussion and advice on m<sup>6</sup>A RIP and bioinformatics analyses, respectively. W.X., H.S. and Y.S. conceived the project and co-wrote the manuscript. H.S. and Y.S. directed all the experiments with input from Y.G.S.

**Competing interest declaration**

Y.S. is a co-founder and holds equity of Constellation Pharmaceuticals, Inc. and Athelas Therapeutics, Inc. Y.S. also holds equity of Imago Biosciences and is a consultant for Active Motif, Inc.

Correspondence and requests for materials should be addressed to Y.S. (yang.shi@ludwig.ox.ac.uk) or H.S. (hongjieshen@fudan.edu.cn).

**Data availability**

The next-generation-sequencing data generated by this study have been deposited to GEO database under accession number GEO: GSE126243.

**Extended Data Fig. 1. METTL3 binds endogenous retroviral elements**

a: Accumulative plots showing the relative distances between peaks of METTL3 and histone modifications.

b: Bar graph showing the overlapping ratios (calculated as Jaccard statistics, see Methods) of METTL3 peaks with repetitive elements.

c: Accumulative plots showing the relative distances between METTL3 peaks and repetitive elements.

d: Heatmaps showing enrichment of METTL3, H3K9me3 and H4K20me3 on repetitive elements.

e: Scatter plots showing the correlation between the enrichment levels of METTL3 and H3K9me3 (Left) or H4K20me3 (Right) on different subtypes (n=277) of ERVK retrotransposons. Two-sided Pearson's correlation test.

f: Schematic representation of stitching adjacent IAPez fragments.

g: Aggregation plots showing METTL3, H3K9me3, H4K20me3 and Input patterns on IAPez-int.

h: Validation of METTL3 binding on IAPez using three independent METTL3 antibodies. The mean of three biological replicates  $\pm$  s.d. is shown.

i: Schematic representation of uniquely mapped reads and randomly mapped un-unique reads.

j: Aggregation plots and heatmaps showing enrichment of METTL3, H3K9me3 and H4K20me3 on the IAPez-int elements with only uniquely mapped reads or uniquely+randomly mapped reads.

Uniquely mapped ChIP-seq reads were used in panel a, b, c, e. Uniquely and randomly mapped ChIP-seq reads were used in panel d, g.

Heatmaps were ranked according to METTL3 enrichment in parental cells in descending order (j).

MTA and MaSat used in ChIP-qPCR are examples of repetitive elements unbound by METTL3.

**Extended Data Fig. 2. METTL3 is required for heterochromatin formation**

a: Western blots showing METTL3 protein levels in parental, *Mettl3* KO and rescued cell lines with METTL3<sup>WT</sup> or METTL3<sup>APPA</sup>.

b: Bar plots showing m<sup>6</sup>A/A ratio on polyA RNAs in parental, *Mettl3* KO and rescued cell lines with METTL3<sup>WT</sup> or METTL3<sup>APPA</sup>. The mean of three biological replicates  $\pm$  s.d. is shown.

c: ChIP-qPCR showing binding patterns of H3K9me3 (Left) and H4K20me3 (Right) on IAPeZ-int elements in parental, *Mettl3* KO and rescued cell lines with METTL3<sup>WT</sup> or METTL3<sup>APPA</sup>. The mean of three biological replicates  $\pm$  s.d. is shown in ChIP-qPCR. \* $p$  < 0.05, \*\* $p$  < 0.01. two-sided t-test. Exact  $p$  values are provided in the Source Data.

d: Boxplots showing enrichment levels of H3K9me3 (Left) and H4K20me3 (Right) on IAPeZ-int elements (n=2,542) in parental, *Mettl3* KO and rescued cell lines with wildtype or catalytically mutated METTL3. \*\*\*\* $p$  < 0.0001 (Exact  $p$  values from left to right: 0, 0, 0, 1.1e-118, 6.2e-269, 0), two-sided paired t-test.

e: Aggregation plots showing enrichment levels of H3K9me3 (Left) and H4K20me3 (Right) on IAPeZ-int elements in parental, *Mettl3* KO and rescued cell line.

f-h: Heatmaps (f), boxplots (g) and aggregation plots (h) showing enrichment levels of H3K9me3 on IAPeZ-int elements (n=2,542) in parental and *Alkbh5* KO cell lines. \*\*\*\* $p$  < 0.0001, two-sided paired t-test.

i: Western blots showing ALKBH5 protein levels in parental and *Alkbh5* KO cell lines.

j-k: Boxplot showing density fold changes ( $\log_2(\text{Mettl3 KO/Parental})$ ) of H3K9me3 (i) and H4K20me3 (j) on different types of repetitive elements upon *Mettl3* KO.  $p$  = 0.00014, two-sided paired t-test.

Uniquely mapped ChIP-seq reads were used in panel d, f, g, j, k. Uniquely+randomly mapped ChIP-seq reads were used in panel e, h.

Heatmaps were ranked according to METTL3 density in parental cells in descending order (f). For the boxplots in panel d, g, j, k, the middle line, lower and upper hinge of the boxplot correspond to the median, the first and third quartiles, respectively. The whiskers extend from the hinges to no further than  $1.5 \times \text{IQR}$  (inter-quartile range) from the hinge. Outlying points that are plotted individually.

For blots, representative of two independent experiments in panel a, i. For blots source data, see Supplementary Figure 1.

MTA and MaSat used in ChIP-qPCR are examples of repetitive elements unbound by METTL3.

**Extended Data Fig. 3. METTL3 is required for heterochromatin formation**

a: Boxplots showing enrichment levels of H3.3 on IAPEz-int elements (n=2,542) in parental, *Mettl3* KO and rescued cell lines with METTL3<sup>WT</sup> or METTL3<sup>APPA</sup>. \*\*\*\*  $p < 0.0001$  (exact  $p$  values from left to right: 4.2e-218, 2.7e-274, 3.9e-294), two-sided paired t-test.

b: Boxplots showing CpG methylation ratios on IAPEz-int elements (n=2,542) in parental, *Mettl3* KO and rescued cell lines with METTL3<sup>WT</sup> or METTL3<sup>APPA</sup>. \*\*\*\*  $p < 0.0001$  (exact  $p$  values from left to right: 4.87e-111, 1.5e-150, 3.9e-294,0), two-sided paired t-test.

c: Boxplot showing density fold changes ( $\log_2(\text{Mettl3 KO/Parental})$ ) of H3.3 on different types of repetitive elements upon *Mettl3* KO.

d: Boxplot showing CpG methylation changes on different types of repetitive elements upon *Mettl3* KO. Only elements with at least 10 covered CpGs were used.

e: RT-qPCR showing RNA levels of IAPEz-int in parental, *Mettl3* KO and rescued cell lines with METTL3<sup>WT</sup> or METTL3<sup>APPA</sup>. The mean of three replicates  $\pm$  s.d. is shown. \*  $p < 0.05$ , \*\*  $p < 0.01$ , two-sided t-test. Exact  $p$  values are provided in the Source Data.

f: Boxplot showing density fold changes ( $\log_2(\text{Mettl3 KO/Parental})$ ) of RNAs of different types of repetitive elements upon *Mettl3* KO.

g-j: Scatter plots showing correlation between METTL3 (g), H3K9me3 (h), H4K20me3 (i), DNA methylation (j) and RNA expression level on IAPEz-int (n=2,542). Two-sided Pearson's correlation test.

k: Boxplot showing RNA levels of the IAPEz-int (n=2,542) in parental, *Mettl3* KO and *Ythdf1/2/3* KO cell lines revealed by PolyA RNA-seq (GSE147849). \*\*\*\*  $p < 0.0001$  (exact  $p$  values from left to right: 1.1e-52, 7.3e-37), two-sided paired t-test.

Uniquely mapped ChIP-seq reads were used in panel a, b, c, d, f, g, h, i, j, k.

For the boxplots in panels a, b, c, d, f and k, the middle line, lower and upper hinge of the boxplot correspond to the median, the first and third quartiles, respectively. The whiskers extend from the hinges to no further than  $1.5 \times \text{IQR}$  (inter-quartile range) from the hinge. Outlying points that are plotted individually.

**Extended Data Fig. 4. METTL3 chromatin binding is dependent on its own catalytic activity**

a: ChIP-qPCR showing binding patterns of METTL3 on IAPeZ-int elements in parental, *Mettl3* KO and rescued cell lines with METTL3<sup>WT</sup> or METTL3<sup>APPA</sup>. The mean of three biological replicates  $\pm$  s.d. is shown. \*  $p < 0.05$ , \*\*  $p < 0.01$ , two-sided t-test. Exact  $p$  values are provided in the Source Data.

b: Aggregation plots showing METTL3 enrichment levels on IAPeZ-int in parental, *Mettl3* KO and rescued cell lines with METTL3<sup>WT</sup> or METTL3<sup>APPA</sup>.

c: Western blot showing interactions of METTL14 with reintroduced METTL3 (METTL3<sup>WT</sup> or METTL3<sup>APPA</sup>) in *Mettl3* KO cells.

d: Aggregation plots showing METTL3 enrichment levels on IAPeZ-int in *Mettl3* KO rescued cells with METTL3<sup>WT</sup>, METTL3<sup>W475A</sup> or METTL3<sup>N477A</sup>.

e: Western blot showing METTL3 protein levels in parental, *Mettl3* KO and rescued cell lines with METTL3<sup>WT</sup>, METTL3<sup>APPA</sup>, METTL3<sup>W475A</sup> or METTL3<sup>N477A</sup>.

f: Aggregation plots showing METTL3 enrichment levels on IAPeZ-int in parental and *Mettl14* KO cell lines.

g: Western blots showing METTL14 protein levels in parental and *Mettl14* KO cell lines.

h: Aggregation plots showing METTL3 enrichment levels on IAPeZ-int in parental and *Rbm15/15b* DKO cell lines.

i: Western blots showing RBM15 and RBM15B protein levels in parental and *Rbm15/15b* DKO cell lines.

j: Aggregation plots showing METTL3 enrichment levels on IAPeZ-int in control and m<sup>6</sup>A methyltransferase complex components KD cell lines.

k: Western blots showing protein levels of m<sup>6</sup>A methyltransferase complex components in control and KD cell lines.

l: A cartoon illustrating the dCas9-METTL3 tethering assay in *Mettl3* KO cell lines.

m: Western blot showing Cas9 and METTL3 protein levels upon Dox treatment.

n: ChIP-qPCR of Cas9 (Left) and H3K9me3 (Right) on IAPeZ and control regions. The mean of three biological replicates  $\pm$  s.d. is shown. \*  $p < 0.05$ , \*\*  $p < 0.01$ , two-sided t-test. Exact  $p$  values are provided in the Source Data.

Uniquely+randomly mapped ChIP-seq reads were used in panel b, d, f, h, j.

For blots, representative of two independent experiments in panel c, e, g, i, k, m. For blots source data, see Supplementary Figure 1.

MTA and MaSat used in ChIP-qPCR are examples of repetitive elements unbound by METTL3.

**Extended Data Fig. 5. METTL3 regulates SETDB1/ TRIM28 recruitment**

a: Venn diagram showing overlaps of the IAPEz elements bound by METTL3, SETDB1 and TRIM28.

b: Scatter plots showing correlation of METTL3 and SETDB1 (Left) or TRIM28 (Right) on IAPEz-int elements (n=2,542). Two-sided Pearson's correlation test.

c: Boxplots showing SETDB1 (Left) and TRIM28 (Right) enrichment levels on the IAPEz-int elements in parental and *Mettl3* KO cell lines.  $p=0$  (Left),  $p=0$  (Right), two-sided paired t-test.

d: ChIP-qPCR showing binding patterns of SETDB1 (Left) and TRIM28 (Right) on IAPEz-int elements in parental and *Mettl3* KO cells. The mean of three biological replicates  $\pm$  s.d. is shown. \*  $p<0.05$ , \*\*  $p<0.01$ , two-sided t-test. Exact  $p$  values are provided in the Source Data.

e-f: Boxplots showing density fold changes ( $\log_2(\text{Mettl3 KO/Parental})$ ) of SETDB1 (e) and TRIM28 (f) on different types of repetitive elements upon *Mettl3* KO.

g: Co-immunoprecipitation coupled western blot showing interactions of SETDB1 (Left) and TRIM28 (Right) with reintroduced METTL3 (wildtype or catalytically mutated) in *Mettl3* KO cells with or without Triptolide treatment.

Uniquely mapped ChIP-seq reads were used in panel b, c, e, f.

For the boxplots in panel c, e and f, the middle line, lower and upper hinge of the boxplot correspond to the median, the first and third quartiles, respectively. The whiskers extend from the hinges to no further than  $1.5 \times \text{IQR}$  (inter-quartile range) from the hinge. Outlying points that are plotted individually.

For blots, representative of two independent experiments in panel g. For blots source data, see Supplementary Figure 1.

**Extended Data Fig. 6. m<sup>6</sup>A exists on IAPEz-int transcripts**

a: RT-qPCR showing relative levels of IAPEz and control RNAs including *Actin* and *Gapdh* in different subcellular populations. The mean of three biological replicates  $\pm$  s.d. is shown.

b: Aggregation plot showing IAPEz-int ChIRP signals enriched on the IAPEz-int elements in the genome.

c: Aggregation plot showing in situ ligated DNA of IAPEz-int transcripts revealed by GRID-seq (GSE82312) enriched on the IAPEz-int elements in the genome.

d: Consensus motif of m<sup>6</sup>A enriched sites (chromatin ribominus RNA).

e: Aggregation plot showing the average enrichment levels of m<sup>6</sup>A ( $\log_2(\text{m}^6\text{A}/\text{input})$ ) over coding genes in parental and *Mettl3* KO cell lines (chromatin ribominus RNA).

f: UCSC snapshots showing m<sup>6</sup>A enrichment at the 3' end of coding genes, which is depleted in the *Mettl3* KO cell lines.

g: Western blots showing SETDB1 protein levels in parental and *Setdb1* CKO cell lines.

h: UCSC snapshots showing m<sup>6</sup>A enrichment at the 5' end of IAPEz-int, which is depleted in the *Mettl3* KO cells.

i: In vitro methyltransferase activity of the METTL3/METTL14 with 20-nucleotide RNA substrates containing four repeats of the consensus sequence. The mean of three biological replicates  $\pm$  s.d. is shown.

Uniquely mapped MeRIP-seq reads were used in panel d, e, f, h. Uniquely+Randomly mapped ChIRP-seq reads and GRID-seq reads were used in panel b, c.

For blots, representative of two independent experiments in panel g. For blots source data, see Supplementary Figure 1.

**Extended Data Fig. 7. YTHDC1's recruitment to IAPEz chromatin depends on its m<sup>6</sup>A recognition ability**

a: ChIP-qPCR showing enrichment levels of nuclear localized m<sup>6</sup>A reader proteins. The mean of three biological replicates  $\pm$  s.d. is shown.

b: Venn diagram showing overlaps between METTL3 and YTHDC1 binding events.

c: Scatter plot showing correlation of METTL3 and YTHDC1 on IAPEz-int elements.

d-e: UCSC snapshot (d) and ChIP-qPCR (e) showing YTHDC1 enrichment on the IAPEz-int elements in parental, *Mettl3* KO and rescued cell lines with wildtype or catalytically mutated METTL3. The mean of three biological replicates  $\pm$  s.d. is shown. \*  $p < 0.05$ , \*\*  $p < 0.01$ , two-sided t-test. Exact  $p$  values are provided in the Source Data.

f: Construction of YTHDC1<sup>WT</sup>, *Ythdc1* KO, and YTHDC1<sup>W429A</sup> cell lines using an auxin-inducible degron (AID) system.

g: Western blots showing IAA-induced rapid degradation of AID-YTHDC1.

h-k: Heatmaps (h), UCSC snapshots (i), Boxplots (j) and Aggregation plots (k) showing YTHDC1 levels on IAPEz-int in YTHDC1<sup>WT</sup>, *Ythdc1* KO, and YTHDC1<sup>W429A</sup> cell lines. \*\*\*\*  $p < 0.0001$  (Exact  $p$  values from left to Right: 0, 0), two-sided paired t-test.

l: ChIP-qPCR showing YTHDC1 enrichment levels on the IAPEz-int elements in control mESCs and mESCs treated with  $\alpha$ -amanitin, flavopiridol and triptolide, respectively. The mean of three biological replicates  $\pm$  s.d. is shown. \*  $p < 0.05$ , \*\*  $p < 0.01$ . two-sided t-test. Exact  $p$  values are provided in the Source Data.

Uniquely mapped ChIP-seq reads were used in panel b, c, d, h, i, j. Uniquely+randomly mapped ChIP-seq reads were used in panel k.

Heatmaps were ranked according to METTL3 density in parental cells in descending order in panel h.

For the boxplots in j, the middle line, lower and upper hinge of the boxplot correspond to the median, the first and third quartiles, respectively. The whiskers extend from the hinges to no further than  $1.5 \times \text{IQR}$  (inter-quartile range) from the hinge. Outlying points that are plotted individually.

For blots, representative of two independent experiments in panel g. For blots source data, see Supplementary Figure 1.

MTA and MaSat used in ChIP-qPCR are examples of repetitive elements unbound by METTL3.

**Extended Data Fig. 8. YTHDC1 stabilizes METTL3 on heterochromatin**

a-c: Boxplots (a), and Aggregation plots (b), and UCSC snapshot (c) showing METTL3 levels on IAPeZ-int in YTHDC1<sup>WT</sup>, *Ythdc1* KO and YTHDC1<sup>W429A</sup> cell lines. \*\*\*\*  $p < 0.0001$  (Exact  $p$  values from left to Right:  $2.3 \times 10^{-176}$ ,  $1.2 \times 10^{-195}$ ), two-sided paired t-test.

d-f: Boxplots (d), and Aggregation plots (e), and UCSC snapshot (f) showing H3K9me3 levels on IAPeZ-int in YTHDC1<sup>WT</sup>, *Ythdc1* KO and YTHDC1<sup>W429A</sup> cell lines. \*\*\*\*  $p < 0.0001$  (Exact  $p$  values from left to Right:  $7.1 \times 10^{-63}$ ,  $4.8 \times 10^{-279}$ ), two-sided paired t-test.

g-j: Heatmaps (g), and boxplots (h), and Aggregation plots (i), and UCSC snapshots (j) showing H4K20me3 levels on IAPeZ-int in YTHDC1<sup>WT</sup>, *Ythdc1* KO and YTHDC1<sup>W429A</sup> cell lines. \*\*\*\*  $P < 0.0001$  (Exact  $p$  values from left to Right:  $8.8 \times 10^{-30}$ ,  $7.8 \times 10^{-114}$ ), two-sided paired t-test.

k: Western blots showing protein levels of METTL3 and YTHDC1 in control, *Mettl3* KO, *Ythdc1* KD and *Mettl3* KO+*Ythdc1* KD cell lines.

l: ChIP-qPCR showing H3K9me3 enrichment level on METTL3 elements in control, *Mettl3* KO, *Ythdc1* KD and *Mettl3* KO+*Ythdc1* KD cell lines. \*  $p < 0.05$ , \*\*  $p < 0.01$ . two-sided t-test. Exact  $p$  values are provided in the Source Data.

m: Western blots showing Cas9 protein levels upon Dox treatment in *Mettl3* KO cell lines.

n: ChIP-qPCR of H3K9me3 (Left) and Cas9 (Right) on IAP and control regions in *Mettl3* KO cell lines expressing dCas9-YTHDC1. The mean of three biological replicates  $\pm$  s.d. is shown. \*  $p < 0.05$ , \*\*  $p < 0.01$ . two-sided t-test. Exact  $p$  values are provided in the Source Data.

o: Western blots showing Cas9 and METTL3 protein levels upon Dox treatment in *Mettl3* KO+METTL3<sup>APPA</sup> cell lines.

p: ChIP-qPCR of H3K9me3 (Left) and Cas9 (Right) on IAP and control in *Mettl3* KO+METTL3<sup>APPA</sup> cell lines expressing dCas9-YTHDC1. The mean of three biological replicates  $\pm$  s.d. is shown. Exact  $p$  values are provided in the Source Data.

q: Co-immunoprecipitation coupled with western blots showing interactions of YTHDC1 with reintroduced METTL3 (wildtype or catalytically mutated) in *Mettl3* KO cells with or without Triptolide treatment.

Uniquely mapped ChIP-seq reads were used in panel a, c, d, f, g, h, j. Uniquely+randomly mapped ChIP-seq reads were used in panel b, e, i.

Heatmaps were ranked according to METTL3 density in parental cells in descending order in panel g.

For the boxplots in panel a, d, h, the middle line, lower and upper hinge of the boxplot correspond to the median, the first and third quartiles, respectively. The whiskers extend from the hinges to no further than  $1.5 \times$  IQR (inter-quartile range) from the hinge. Outlying points that are plotted individually.

For blots, representative of two independent experiments in panel k, m, q. For blots source data, see Supplementary Figure 1.

MTA and MaSat used in ChIP-qPCR are examples of repetitive elements unbound by METTL3.

**Extended Data Fig. 9. SETDB1 regulates METTL3/ YTHDC1 recruitment**

a-d: Heatmaps (a), UCSC snapshot (b), boxplot (c) and aggregation plots (d) showing METTL3 enrichment levels on IAPez-int in parental and *Setdb1* CKO cells.  $p$  value =  $1.3\text{e-}48$ , two-sided paired t-test.

e-h: Heatmaps (e), UCSC snapshot (f), boxplot (g) and aggregation plots (h) showing YTHDC1 enrichment levels on IAPez-int in parental and *Setdb1* CKO cells.  $p$  value =  $4.5\text{e-}100$ , two-sided paired t-test.

Uniquely mapped ChIP-seq reads were used in panel a, b, c, e, f, g. Uniquely+randomly mapped ChIP-seq reads were used in panel d, h.

Heatmaps were ranked according to METTL3 density in parental cells in descending order in panel a, e.

For the boxplots in panel c, g, the middle line, lower and upper hinge of the boxplot correspond to the median, the first and third quartiles, respectively. The whiskers extend from the hinges to no further than  $1.5 \times \text{IQR}$  (inter-quartile range) from the hinge. Outlying points that are plotted individually.

**Extended Data Fig. 10. RNA dependent heterochromatin formation models**

a. RNA dependent heterochromatin formation on IAPeZ-int in mESC. Specifically, METTL3 together with other m<sup>6</sup>A methyltransferase components methylate IAPeZ transcripts, which are recognized by the m<sup>6</sup>A reader protein YTHDC1. YTHDC1 in turn stabilizes METTL3 binding, possibly through protein-protein interaction. Chromatin associated METTL3 enhances SETDB1/TRIM28 binding, which in turn stabilizes METTL3 recruitment.

b. RNA dependent heterochromatin formation on centromere regions in *S. pombe*. Specifically, heterochromatin generation over centromere regions is initiated by the base-pairing recognition and binding of RITS complex to the RNAs transcribed from these regions, which in turn enhances sRNA generation through recruitment of RDRC. RITS then recruits CLRC to catalyze H3K9 methylation, which in turn promotes RITS binding.

c. RNA dependent heterochromatin formation on DSR genes in *S. pombe*. Specifically, Mmi1 protein recognizes the DSR consensus motif on the RNAs transcribed from these genes and then recruits the H3K9 methyltransferase Clr4 through Red1.

**a** METTL3 peaks

Jaccard overlapping ratio

H3K9me3 H4K20me3 H3K27me3 H3K4me3

**b** METTL3 H3K9me3 H4K20me3

METTL3 peaks sorted by METTL3

-5K center 5K

**c**

IAPA\_MM-Int IAPLTR1a\_MM IAPEx-Int IAPLTR2\_MM IAPLTR1\_MM RMER8-Int MYSERV16\_Int MYSERV4\_19-Int MURERV4\_Mur RLTR22\_Mur RLTR17D\_MM

METTL3 H3K9me3 H4K20me3

5 4 3 2 1 0 -1 -2

**d**

$\log_2(\text{H3K9me3}/\text{Input})$

$\log_2(\text{METTL3}/\text{Input})$

$p = 1.7e-177$   
 $r = 0.72$

**e**

$\log_2(\text{H4K20me3}/\text{Input})$

$\log_2(\text{METTL3}/\text{Input})$

$p = 2.4e-151$   
 $r = 0.68$

**f**

chr2:167,267,330-167,308,129 chr3:14,693,030-14,725,471 chr1:185,047,084-85,081,739

METTL3 3200 1500 1000 1000

H3K9me3 1000 1000 1000

H4K20me3 1200 1500 1000

Input 1000 1000 1000

Fig. 2. METTL3 is required for heterochromatin formation over repetitive elements

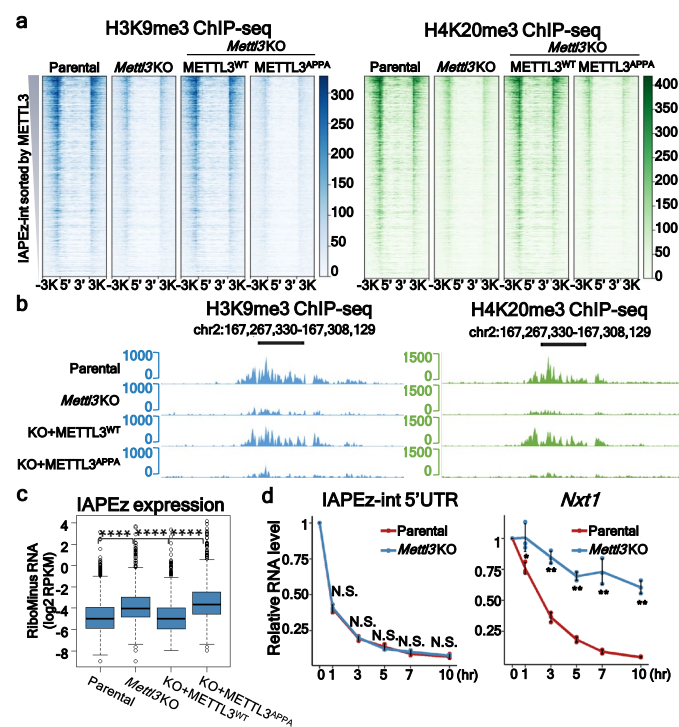
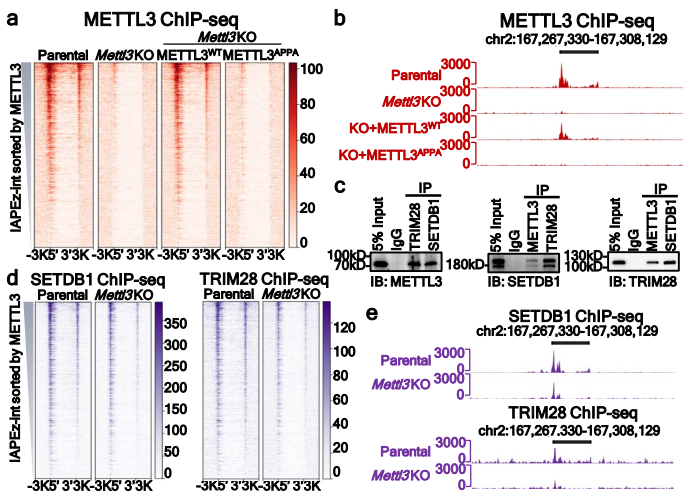
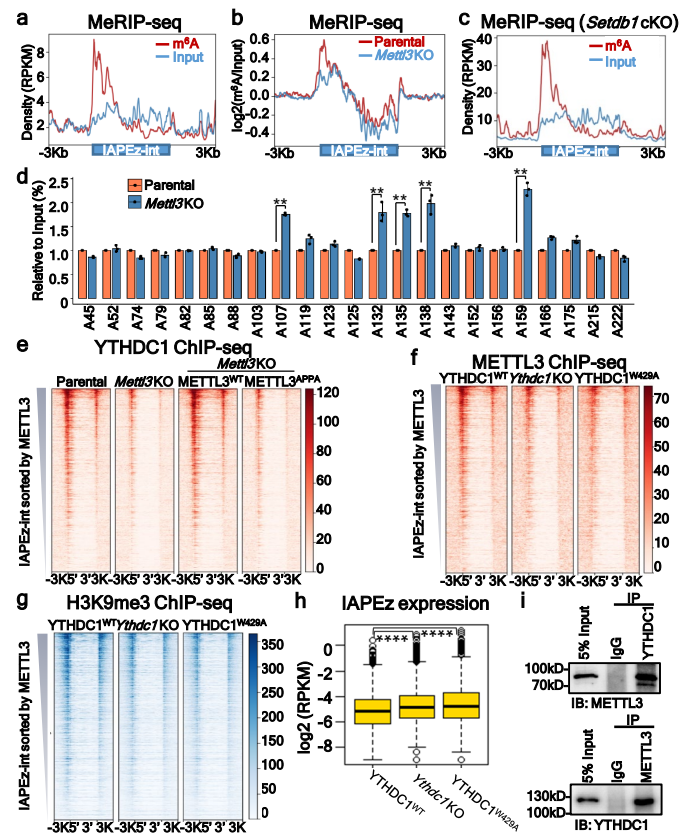


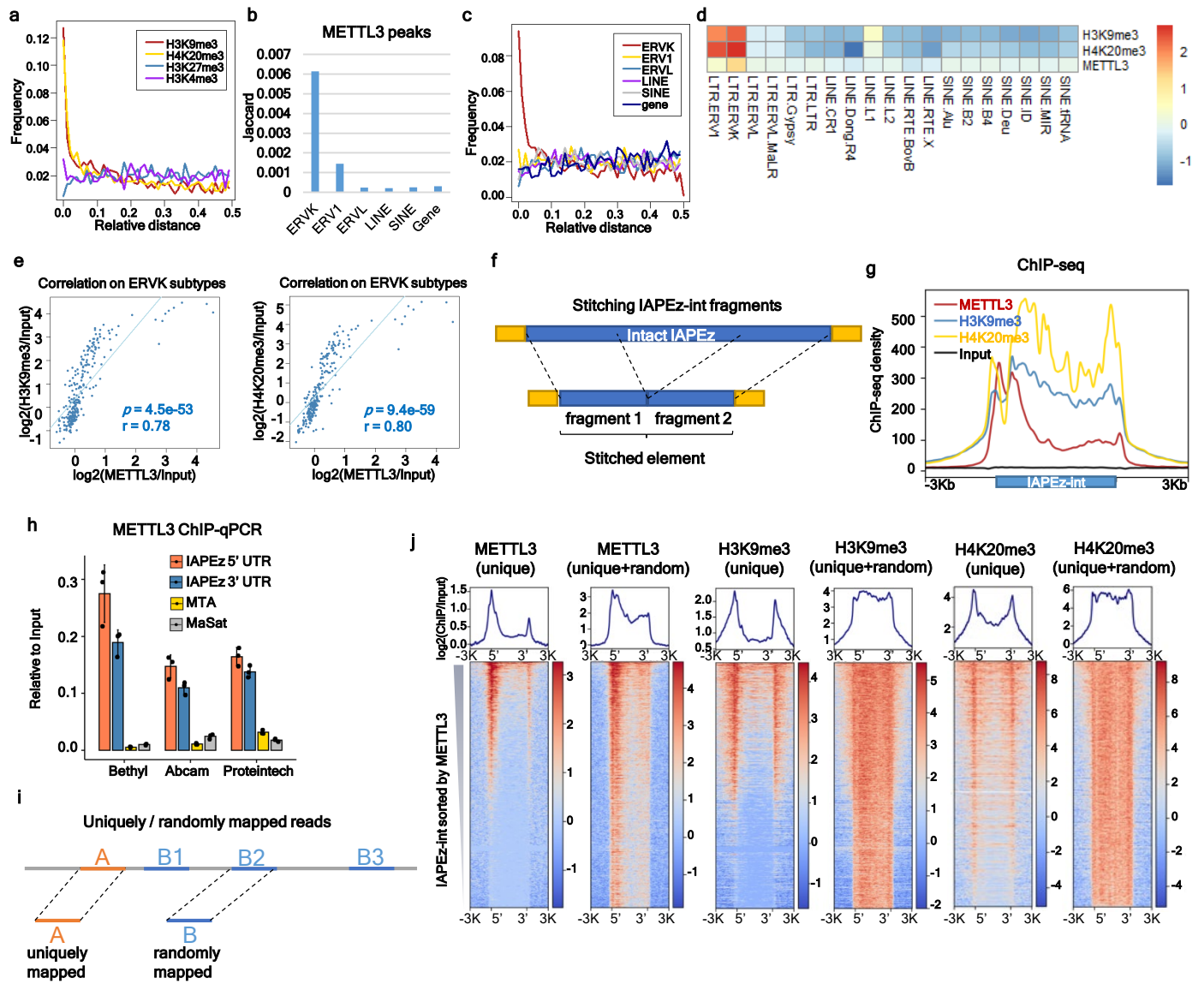
Fig. 3. METTL3 regulates SETDB1/TRIM28 localization to IAPEz elements



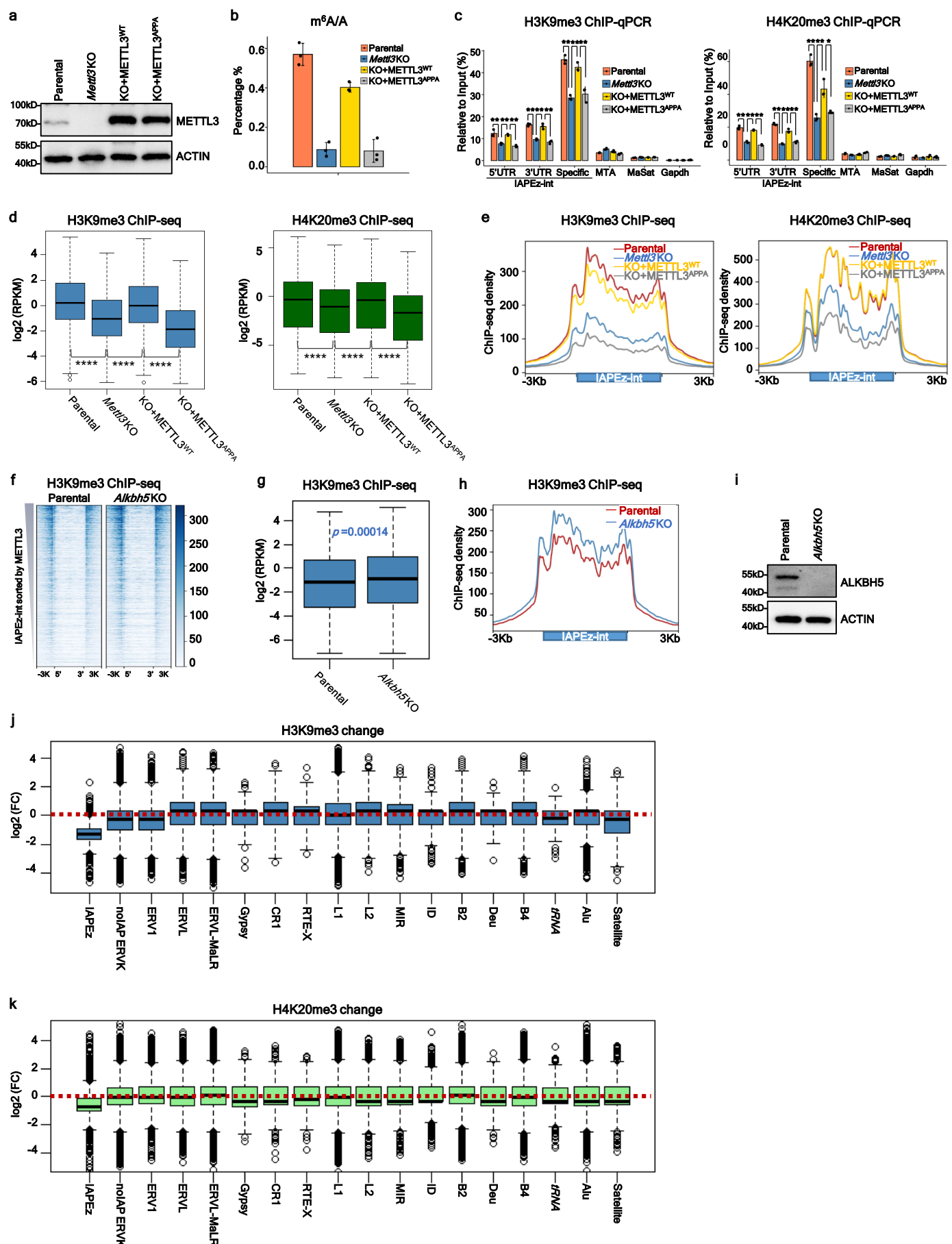
**Fig. 4. YTHDC1 recruited by METTL3 dependent m6A contributes to METTL3 binding and heterochromatin formation on IAPEz-int**



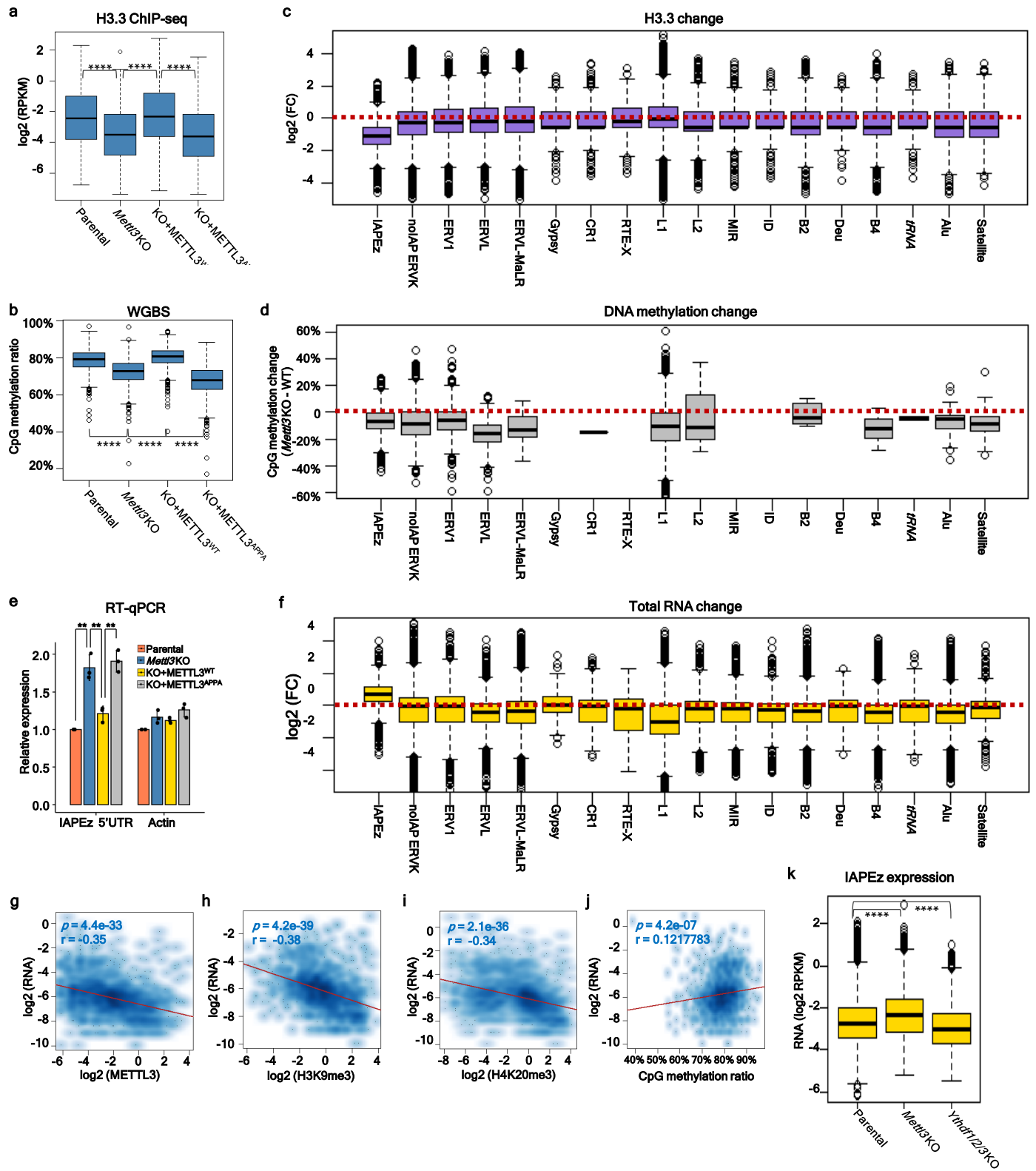
**Extended Data Fig. 1. METTL3 binds endogenous retroviral elements**



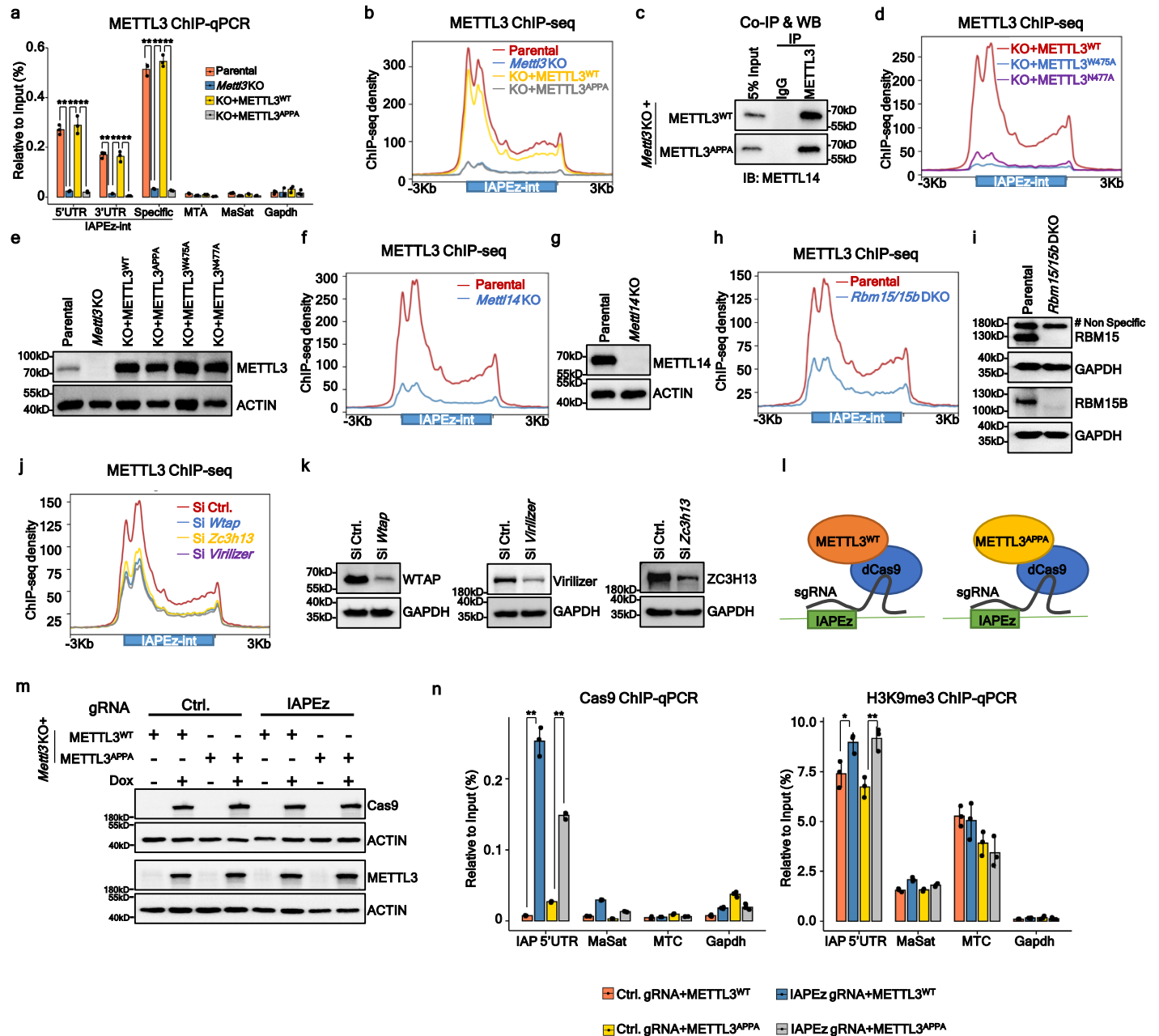
## Extended Data Fig. 2. METTL3 is required for heterochromatin formation



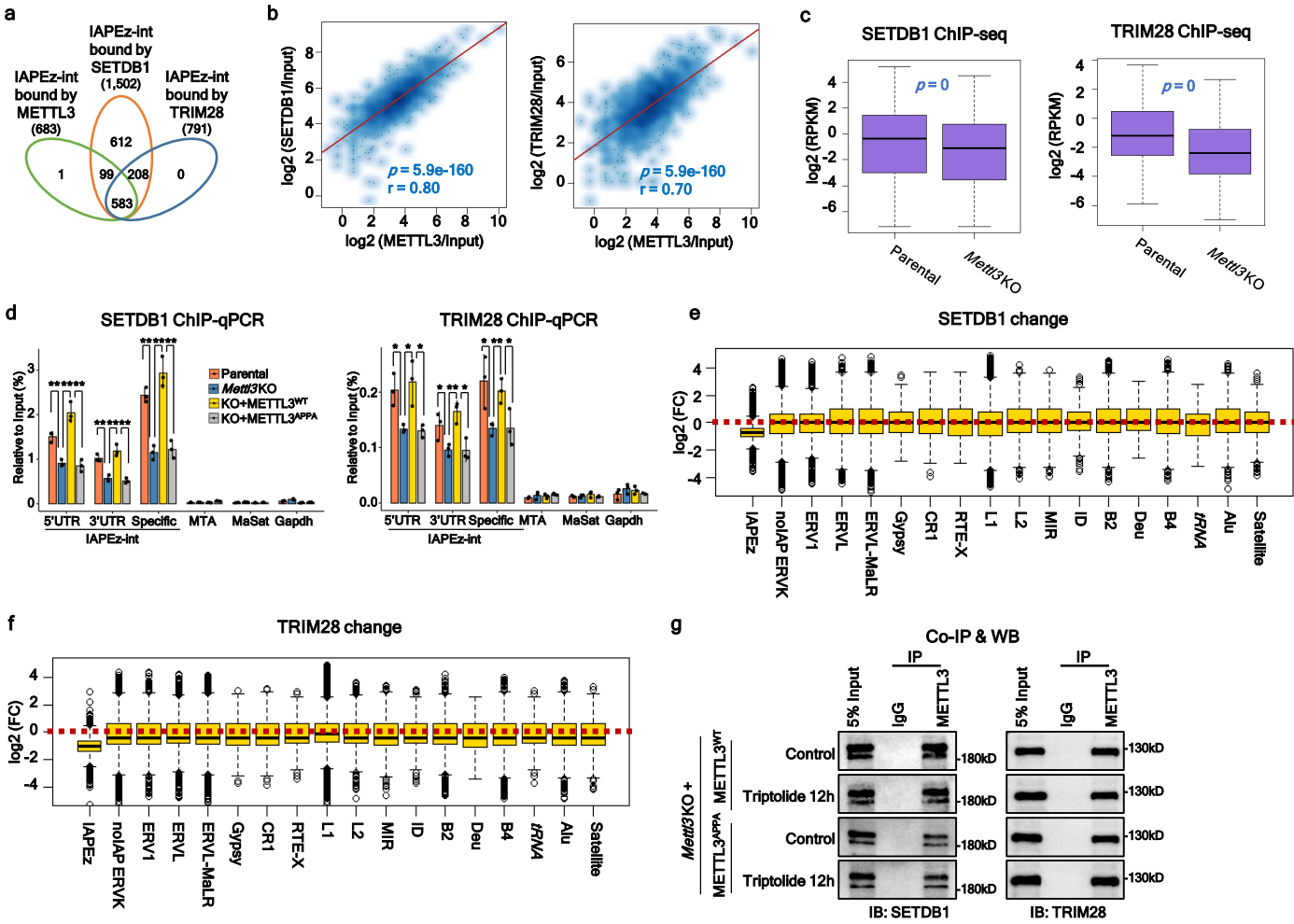
**Extended Data Fig. 3. METTL3 is required for heterochromatin formation**



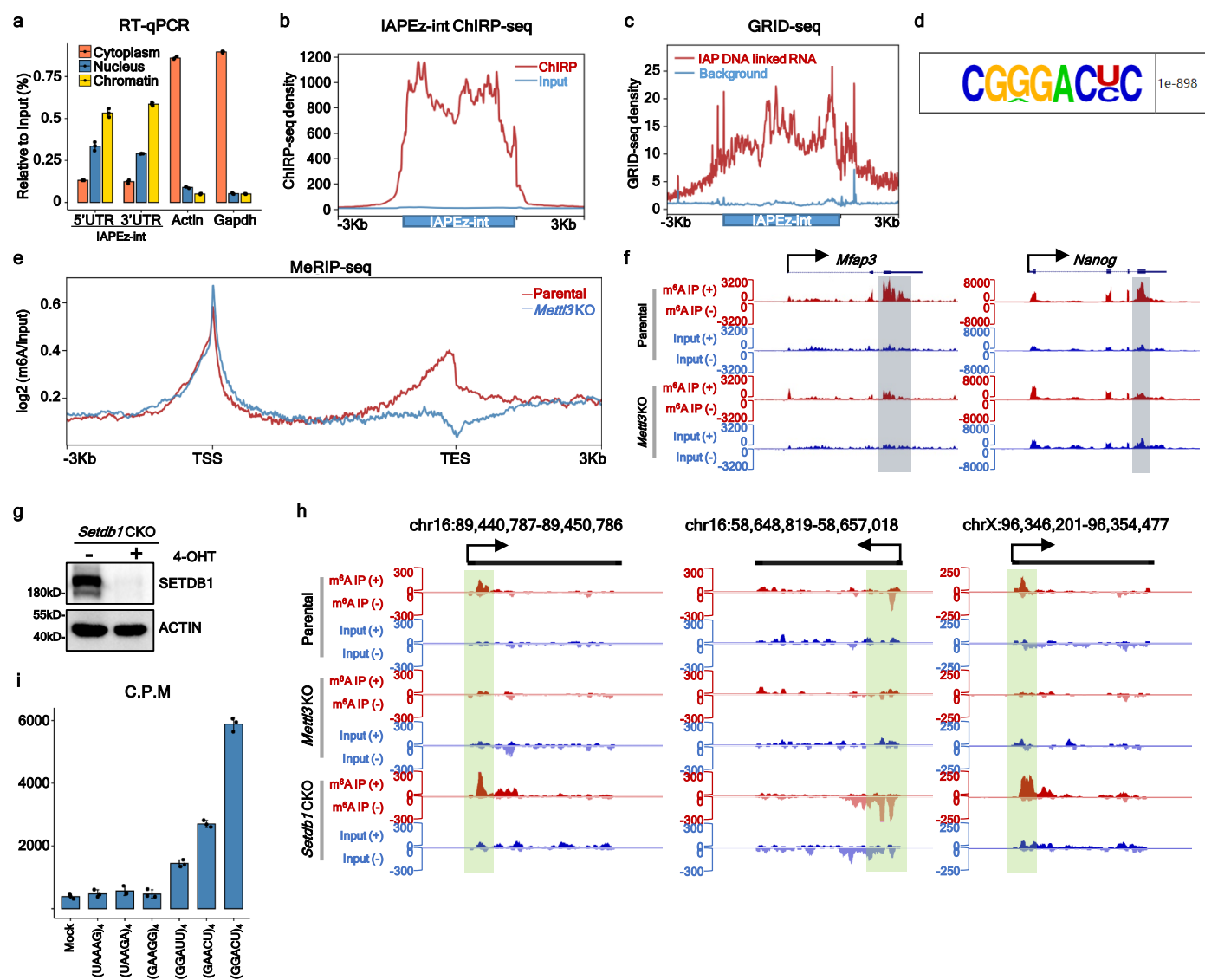
**Extended Data Fig. 4. METTL3 chromatin binding is dependent on its own catalytic activity**



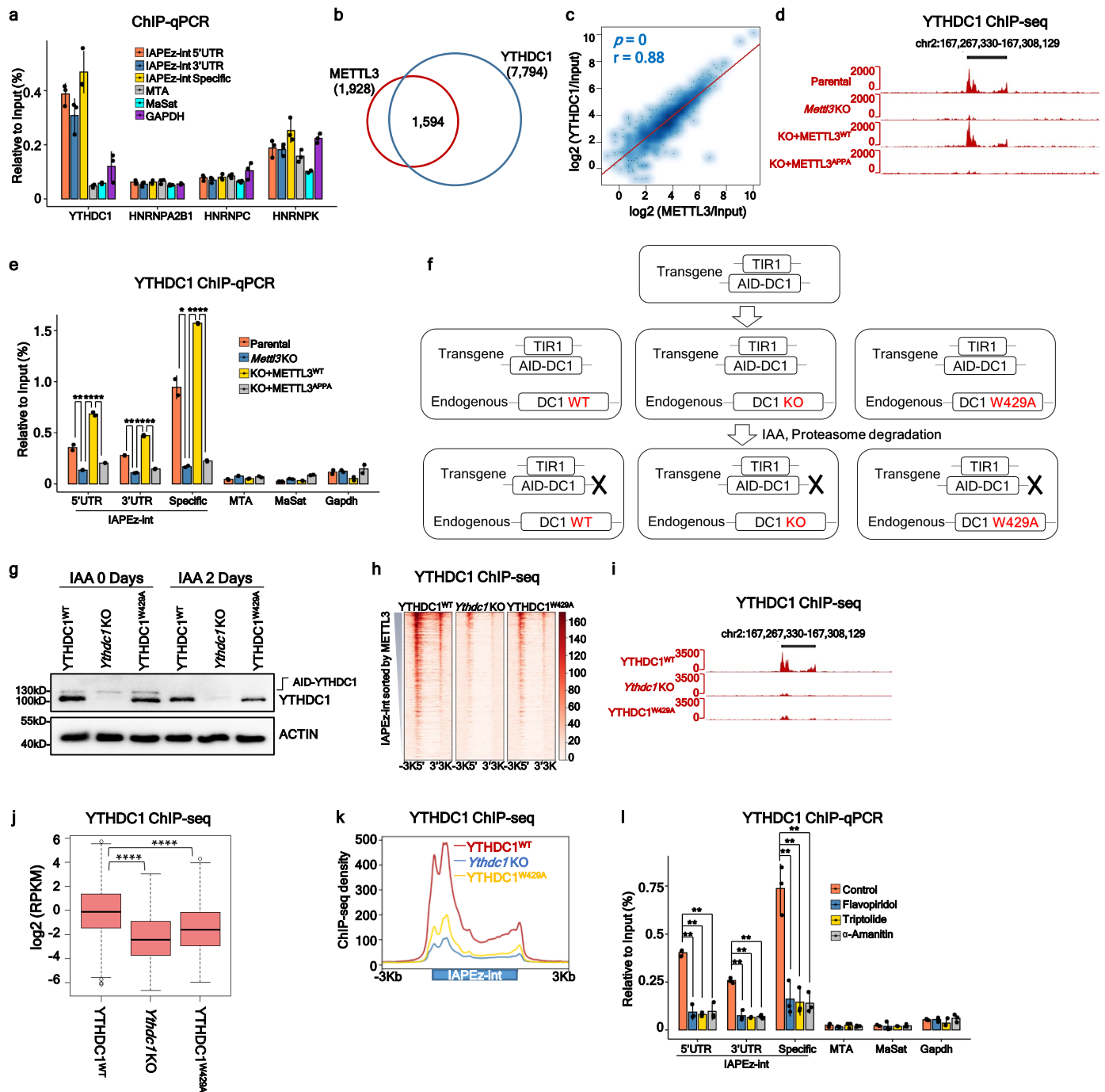
Extended Data Fig. 5. METTL3 regulates SETDB1/ TRIM28 recruitment



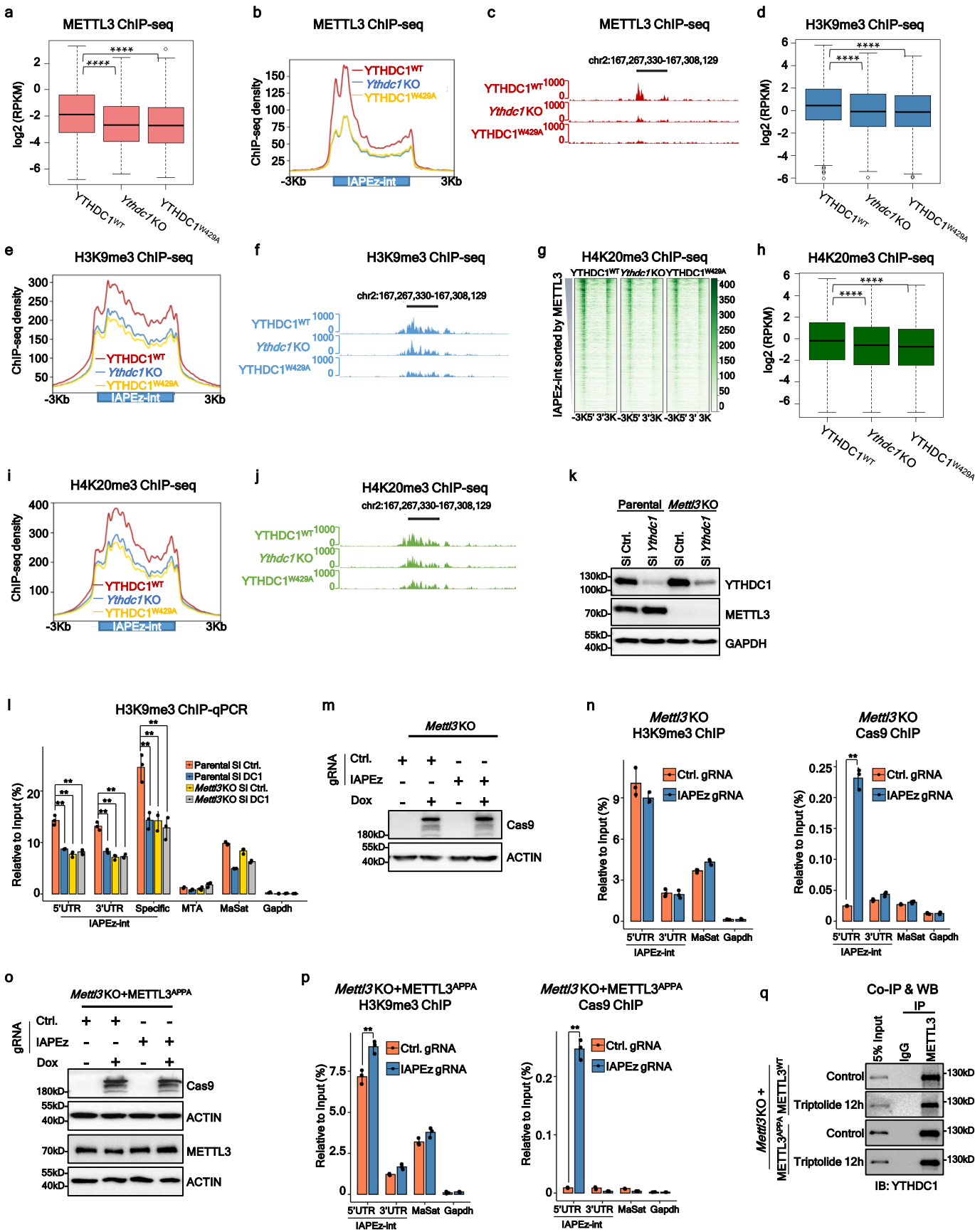
Extended Data Fig. 6. m<sup>6</sup>A exists on IAPez-int transcripts



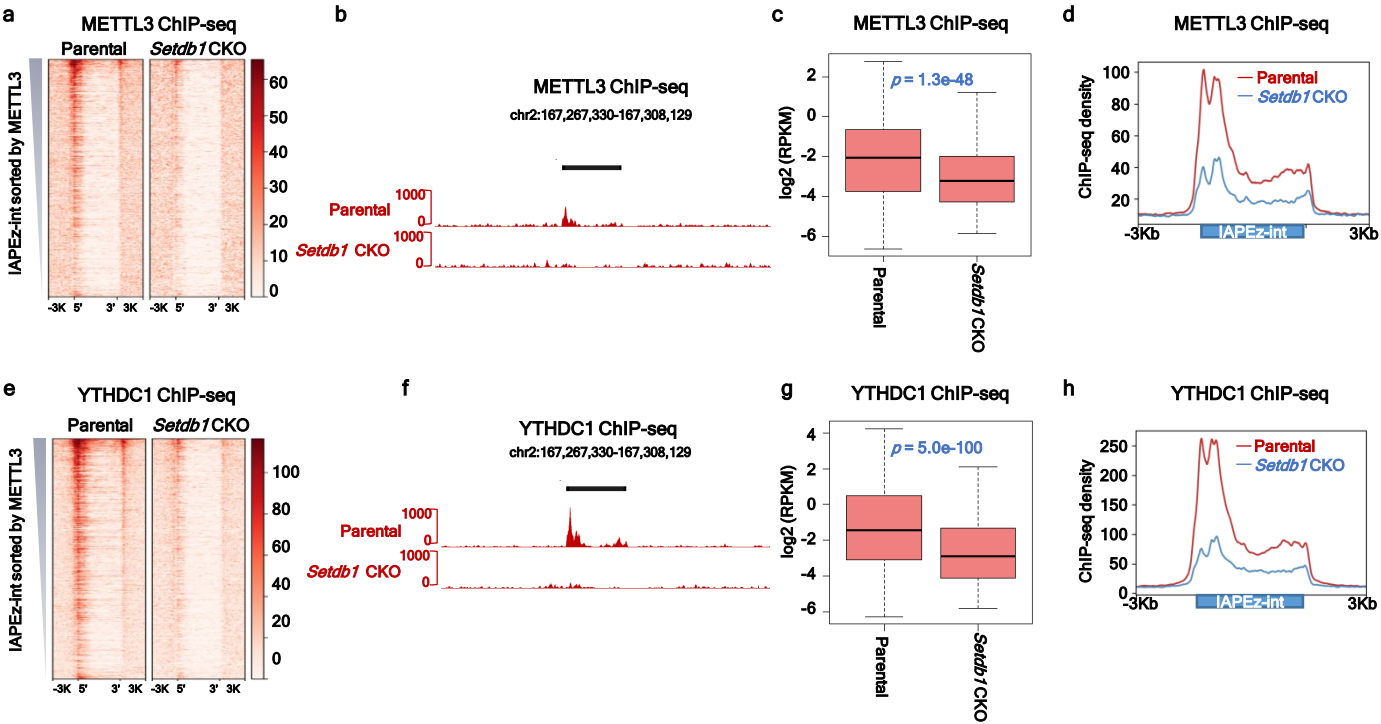
# Extended Data Fig. 7. YTHDC1's recruitment to IAPEz chromatin depends on its m<sup>6</sup>A recognition ability



Extended Data Fig. 8. YTHDC1 stabilizes METTL3 on heterochromatin



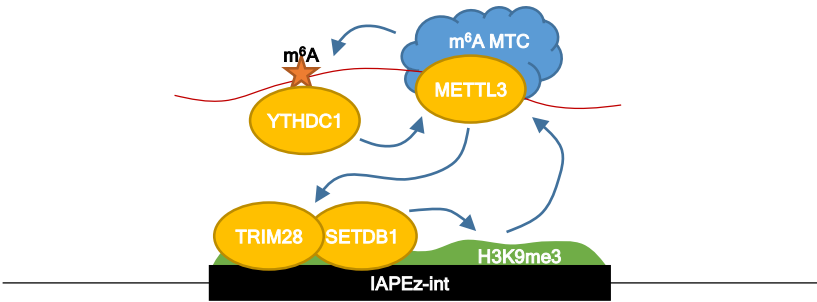
Extended Data Fig. 9. SETDB1 regulates METTL3/ YTHDC1 recruitment



Extended Data Fig. 10. RNA dependent heterochromatin formation models

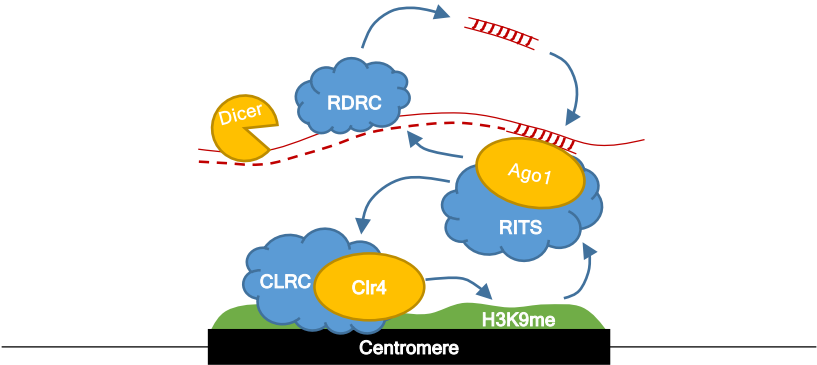
a

*Mus Musculus* (IAPEz elements)



b

*S. Pombe* (Centromere)



c

*S. Pombe* (DSR genes)

